ISSN 1560-3547, Regular and Chaotic Dynamics, 2021, Vol. 26, No. 5, pp. 482–504. © Pleiades Publishing, Ltd., 2021.

# Something Old, Something New: Three Point Vortices on the Plane

**Mark A. Stremler**[1*]

[1]*Department of Biomedical Engineering & Mechanics, Virginia Tech, VA 24061 Blacksburg, USA*

Received June 21, 2021; revised August 12, 2021; accepted August 18, 2021

**Abstract**—The classic problem of three point vortex motion on the plane is revisited by using the interior angles of the vortex triangle, $\theta_j$, $j = 1, 2, 3$, as the key system variables instead of the lengths of the triangle sides, $s_j$, as has been used classically. Similar to the classic approach, the relative vortex motion can be represented in a phase space, with the topology of the level curves characterizing the motion. In contrast to the classic approach, the alternate formulation gives a compact, consistent phase space representation and facilitates comparisons of vortex motion in a co-moving frame. This alternate formulation is used to explore the vortex behavior in the two canonical cases of equal vortex strength magnitudes, $\Gamma_1 = \Gamma_2 = \Gamma_3$ and $\Gamma_1 = \Gamma_2 = -\Gamma_3$.

MSC2010 numbers: 01-02, 37E35, 70F07, 70H06, 76B47, 76-03

**DOI:** 10.1134/S1560354721050038

Keywords: vortex dynamics, point vortices, three-vortex problem, potential flow

## 1. INTRODUCTION

Soon after Hermann Helmholtz introduced the point vortex model [20], Walter Gröbli considered the problem of three point vortices on the plane [10], apparently at the suggestion of Heinrich Weber [6]. This classic problem has been visited and revisited numerous times [1, 3, 6, 7, 12, 15, 16, 18] during the nearly 150 years since Gröbli's original solutions. The longevity of this problem can be attributed to several key features. From a physical perspective, the point vortex system has proven to be a useful reduced-order model of vorticity-dominated flows [15, 19, 21], and the planar three-point-vortex system is the simplest such model that produces time-dependent inter-vortex separations. From a mathematical perspective, the general three vortex problem is integrable but nontrivial, yielding a rich solution space while remaining tractable. This manuscript is the latest addition to the literature on this classic problem, applying a more recent formulation [3, 12] to the general classification of three vortex motion. This formulation provides a consistent, compact phase-plane representation of the relative motion and facilitates defining a useful co-moving frame of reference for investigating and comparing details of the motion.

As a starting point, consider a system consisting of inviscid fluid on the two-dimensional plane that is irrotational everywhere but at three isolated point vortices. The circulation, or strength, of each vortex is given by $\Gamma_j$ (with $j = 1, 2, 3$), and the discussion here assumes that $\Gamma_j \neq 0$. Several symmetric functions of the circulations appear in the various solution methods, namely,

$$\gamma_1 = \Gamma_1 + \Gamma_2 + \Gamma_3, \tag{1.1a}$$

$$\gamma_2 = \Gamma_1\Gamma_2 + \Gamma_2\Gamma_3 + \Gamma_3\Gamma_1, \tag{1.1b}$$

$$\gamma_3 = \Gamma_1\Gamma_2\Gamma_3 \neq 0. \tag{1.1c}$$

It is helpful to introduce the dimensionless strength ratios

$$G_1 = \frac{\Gamma_0}{\Gamma_1}, \quad G_2 = \frac{\Gamma_0}{\Gamma_2}, \quad G_3 = \frac{\Gamma_0}{\Gamma_3}, \tag{1.2}$$

*E-mail: stremler@vt.edu

together with the associated dimensionless symmetric functions

$$g_1 = G_1 + G_2 + G_3 = \Gamma_0 \frac{\gamma_2}{\gamma_3}, \tag{1.3a}$$

$$g_2 = G_1G_2 + G_2G_3 + G_3G_1 = \Gamma_0^2 \frac{\gamma_1}{\gamma_3}, \tag{1.3b}$$

$$g_3 = G_1G_2G_3 = \Gamma_0^3 \frac{1}{\gamma_3}, \tag{1.3c}$$

where $\Gamma_0$ is an arbitrarily chosen characteristic vortex strength. When values are specified in this paper, it will be assumed without any loss of generality that $\Gamma_0 = \Gamma_1$, giving $G_1 = 1$.

The positions of the three vortices can be represented in the complex plane as $z_j = x_j + \mathrm{i}\, y_j$ $(j = 1, 2, 3)$, in which case the equations of motion for the vortices can be written as (see, e. g., Ref. [4])

$$\frac{\mathrm{d}\overline{z_j}}{\mathrm{d}t} = \frac{1}{2\pi\mathrm{i}} \sum_{\substack{k=1 \\ k\neq j}}^{3} \frac{\Gamma_k}{z_j - z_k}, \tag{1.4}$$

where $\overline{z_j} = x_j - \mathrm{i}\, y_j$ is the complex conjugate of $z_j$. Key constants of the motion governed by (1.4) are the linear impulse,

$$Q + \mathrm{i}P = \sum_{k=1}^{3} \Gamma_k z_k, \tag{1.5}$$

and the angular impulse defined with respect to an arbitrary point $z$,

$$I_z = \sum_{k=1}^{3} \Gamma_j \left| z_k - z \right|^2, \tag{1.6}$$

corresponding to translational and rotational invariance of the system, respectively. The center of vorticity, $z_{\mathrm{cv}}$, given by the weighted average of the vortex positions (for $\gamma_1 \neq 0$),

$$z_{\mathrm{cv}} = \frac{\sum_{k=1}^{3} \Gamma_k z_k}{\sum_{k=1}^{3} \Gamma_k} = \frac{Q + \mathrm{i}P}{\gamma_1}, \tag{1.7}$$

is thus also a constant of the motion. When describing the motion of the vortices in terms of the corresponding triangle, as discussed below, an important variation on these constants is the quantity

$$L = \gamma_1 I_0 - Q^2 - P^2 = \gamma_1 I_{\mathrm{cv}} = \sum_{j=1}^{3} \sum_{k>j}^{3} \Gamma_j \Gamma_k \left| z_j - z_k \right|^2, \tag{1.8}$$

where $I_0$ and $I_{\mathrm{cv}}$ are the angular impulse (1.6) defined with respect to $z = 0$ and $z = z_{\mathrm{cv}}$, respectively. This system of equations (1.4) can be written in Hamiltonian form as

$$\Gamma_j \frac{\mathrm{d}\overline{z_j}}{\mathrm{d}t} = \mathrm{i} \frac{\partial \mathcal{H}}{\partial z_j}, \quad j = 1, 2, 3, \tag{1.9a}$$

where

$$\mathcal{H} = -\frac{1}{4\pi} \sum_{j=1}^{3} \sum_{k>j}^{3} \Gamma_j \Gamma_k \log \left( z_j - z_k \right)^2 \tag{1.9b}$$

is the complex continuation of the real-valued Hamiltonian

$$H = \mathrm{Re}(\mathcal{H}) = -\frac{1}{4\pi} \sum_{j=1}^{3} \sum_{k>j}^{3} \Gamma_j \Gamma_k \ln \left| z_j - z_k \right|^2. \tag{1.10}$$

(Note that this presentation corrects the errors in Eqs. (2.6)–(2.7) of Ref. [13].)

Modern numerical tools make it quite straightforward to accurately solve for the time-dependent vortex dynamics directly from Eqs. (1.4). In fact, for all of the vortex trajectories shown as examples in this manuscript, Eqs. (1.4) were integrated in Mathematica (Wolfram Research, Inc.) using the `NDSolve` command. When the sum of the vortex strengths is zero, i. e., $\gamma_1 = 0$ or $g_2 = 0$, the relative vortex motion in this formulation can be reduced to the advection of a passive particle in a field of fixed point vortices in the complex plane [2]. However, classification of the vortex motions for a broad range of system parameters via representation in a phase space has limited application in the complex variable formulation. The full problem for $\gamma_1 \neq 0$ does not have a tractable representation when considered in terms of the complex positions, and an alternative solution approach must be taken.

As shown in Fig. 1, the three vortices can be considered as the vertices of a triangle, and representing the governing equations in terms of the triangle variables enables classification of the relative motion. In Section 2, an overview is given of the classic approach first introduced by Gröbli [10] that uses the lengths of the triangle sides, $s_j$, as the fundamental variables. This formulation does provide a broad classification of the relative vortex motion using the topological structure of level curves in a phase space, but the presentation is somewhat unwieldy, with the phase space variables having case-dependent definitions and the phase space boundary being dependent on the system parameters. In Section 3, an alternative approach is taken that uses the interior angles of the triangle, $\theta_j$, as the fundamental variables. This formulation is applied in Section 4 to two fundamental selections of the vortex strengths, $\Gamma_1 = \Gamma_2 = \pm\Gamma_3$. Appropriate to this special issue, the three-vortex problem with $\Gamma_1 = \Gamma_2 = -\Gamma_3$ was mentioned (without analysis) by Nikolay Zhukovsky in a lecture given to honor von Helmholtz on his seventieth birthday [6]. The significance of taking this new approach to the classic, well-studied problem of planar three-vortex motion is summarized in Section 5.

## 2. THE CLASSIC FORMULATION

Starting with Gröbli [10], studies of the general three-vortex problem [1, 6, 7, 14, 16, 18] have focused on formulating the equations of motion in terms of the inter-vortex separation lengths,

$$s_1 = |z_2 - z_3|\,, \quad s_2 = |z_3 - z_1|\,, \quad s_3 = |z_1 - z_2|\,. \tag{2.1}$$

The reader is referred to, e. g., Refs. [1, 6] for a more comprehensive description of this solution approach; some details are presented here for comparison with the formulation presented in Section 3. The equations of motion (1.4) can be (re)cast as evolution equations for the inter-vortex separations $s_j$, giving [10]

$$\frac{\mathrm{d}s_1^2}{\mathrm{d}t} = \frac{2\Gamma_1\Delta}{\pi}\left(\frac{s_3^2 - s_2^2}{s_3^2 s_2^2}\right), \quad \frac{\mathrm{d}s_2^2}{\mathrm{d}t} = \frac{2\Gamma_2\Delta}{\pi}\left(\frac{s_1^2 - s_3^2}{s_1^2 s_3^2}\right), \quad \frac{\mathrm{d}s_3^2}{\mathrm{d}t} = \frac{2\Gamma_3\Delta}{\pi}\left(\frac{s_2^2 - s_1^2}{s_2^2 s_1^2}\right), \tag{2.2a}$$

where [9]

$$\Delta = \tfrac{1}{16}\left(2s_1^2 s_2^2 + 2s_2^2 s_3^2 + 2s_3^2 s_1^2 - s_1^4 - s_2^4 - s_3^4\right) \tag{2.2b}$$

is the area of the vortex triangle, with $\Delta > 0$ when the vortices are oriented counterclockwise and $\Delta < 0$ when clockwise. In all formulations based on the vortex triangle, colinear configurations with $\Delta = 0$ are singularities of the system. When the problem is cast in terms of the vortex separations $s_j$, the relative motion can be continued through a colinear singularity by evolving the area via [8]

$$\frac{\mathrm{d}\Delta}{\mathrm{d}t} = \frac{1}{8\pi}\left[(\Gamma_1 + \Gamma_2)\,\frac{s_1^2 - s_2^2}{s_3^2} + (\Gamma_2 + \Gamma_3)\,\frac{s_2^2 - s_3^2}{s_1^2} + (\Gamma_3 + \Gamma_1)\,\frac{s_3^2 - s_1^2}{s_2^2}\right]. \tag{2.3}$$

Equations (2.2)–(2.3) form a closed system of ODEs governing the relative motion of the vortices. Various approaches can be taken to then retrieve the full vortex motion in a fixed frame of reference, including integration of the original equations in the complex plane (1.4).

Some vortex motions are relative equilibria, in which case the vortices move together without any changes in their relative positions. These include some colinear configurations and the equilateral triangle configuration. With the form of the governing equations given in (2.2), it is trivial to determine that vortices located at the vertices of an equilateral triangle are in relative equilibrium.

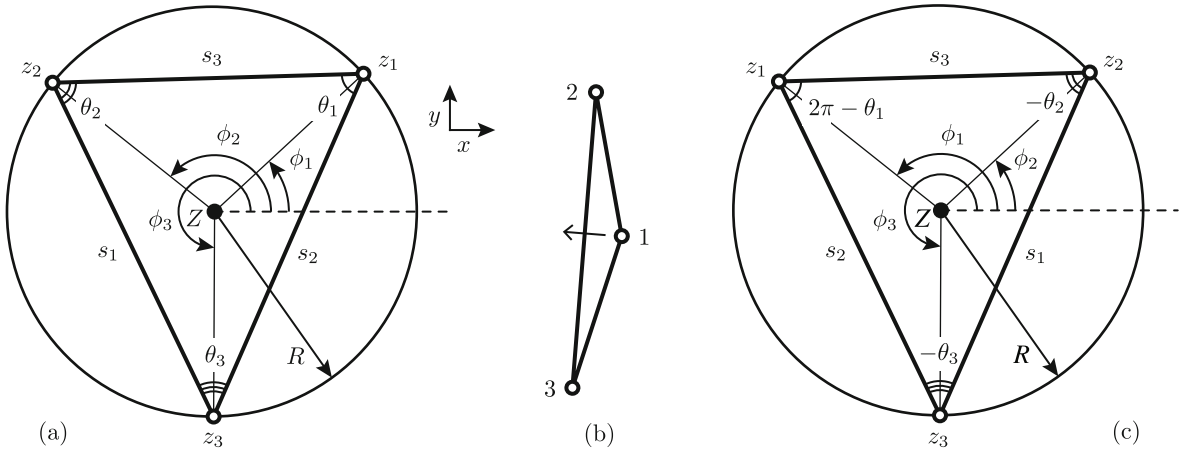


**Fig. 1.** The triangle and circumcircle defined by three point vortices at positions $z_j$ for (a) a counterclockwise orientation and (c) a clockwise orientation of the vortex labels. For comparison with [3, 12, 13], which assume counterclockwise orientation, the interior angles in (a) are related as $\theta_1 = A$, $\theta_2 = B$, $\theta_3 = C$. (b) One of the possible transitions from a counterclockwise to a clockwise orientation, which relates the $\theta_j$ definitions in (a) and (c).

For an equilateral triangle, $s_1 = s_2 = s_3$, so that $\mathrm{d}s_j^2/\mathrm{d}t = 0$, and the lengths remain equal for all time. Note that in general this configuration is only in relative equilibrium, not absolute equilibrium; i. e., the triangle will rotate and/or translate with respect to a fixed observer depending on the values of the vortex strengths. The colinear equilibria are more difficult to investigate, as only isolated cases of colinear configurations are in relative equilibrium. A discussion of these configurations is presented in Section 3.4.

If $L \neq 0$, the relative vortex motion can be characterized by substituting (2.1) into (1.8) to obtain

$$b_1 + b_2 + b_3 = 3, \tag{2.4}$$

where the three terms

$$b_j = \frac{3\gamma_3}{L}\left(\frac{s_j^2}{\Gamma_j}\right) = \frac{3\Gamma_0^2}{g_3\, L}\left(G_j s_j^2\right), \quad j = 1, 2, 3, \tag{2.5}$$

can be interpreted as dimensionless *trilinear coordinates* [1], as illustrated in Fig. 2. The regions of the $(b_1, b_2, b_3)$ plane that correspond to physically realizable solutions are constrained by the requirement that the $s_j$ be the lengths of the sides of a triangle; this constraint is equivalent to [1]

$$(\Gamma_1 b_1)^2 + (\Gamma_2 b_2)^2 + (\Gamma_3 b_3)^2 \leqslant 2\left(\Gamma_1\Gamma_2 b_1 b_2 + \Gamma_2\Gamma_3 b_2 b_3 + \Gamma_3\Gamma_1 b_3 b_1\right). \tag{2.6}$$

Boundaries of the "physical regions", determined by the equality in (2.6), are strength-dependent conic sections that are tangent to the trilinear axes [1]. Motions of the vortices must maintain $H =$ constant. Substituting (2.5) into (1.10) and using the notation in (1.2)–(1.3), this constraint can be written as

$$\prod_{j=1}^{3} |b_j|^{G_j} = \exp\left(-4\pi\, g_3\, \frac{H}{\Gamma_0^2}\right)\left|\frac{3\Gamma_0^2}{g_3\, L}\right|^{g_1} \prod_{j=1}^{3} |G_j|^{G_j} = \kappa, \tag{2.7}$$

with $\kappa$ a constant. If $g_1 = 0$ (equivalently, $\gamma_2 = 0$), the constraint becomes independent of the value of $L$ ($\neq 0$).

If instead $L = 0$, then (1.8) can be written as

$$b_1 + b_2 + b_3 = 0, \tag{2.8}$$

with the redefined trilinear coordinates given by

$$b_j = \frac{s_j^2}{\Gamma_j} = \frac{G_j s_j^2}{\Gamma_0}, \quad j = 1, 2, 3. \tag{2.9}$$

The accessible regions of this parameter space are again given by (2.6). Conservation of the Hamiltonian in this case becomes

$$\prod_{j=1}^{3} |b_j|^{G_j} = \exp\left(-4\pi\, g_3 \frac{H}{\Gamma_0^2}\right) |\Gamma_0|^{-g_1} \prod_{j=1}^{3} |G_j|^{G_j} = \kappa_0. \tag{2.10}$$

The $(b_1, b_2, b_3)$ phase space representations for the cases $\Gamma_1 = \Gamma_2 = \pm\Gamma_3$ are shown in Fig. 2; these panels can be compared directly with Figs. 2, 4 and 5 in Ref. [1]. As a vortex motion evolves, the location of that configuration in phase space moves along a level curve of Eq. (2.7) (or Eq. (2.10) if $L = 0$). At the points where level curves intersect the boundary of the physical region, the vortices in the configuration are colinear. The points where a level curve is tangent to the physical boundary correspond to a colinear configuration in relative equilibrium, and these isolated level curves are *separatrices* that delineate different *regimes of motion*. In some cases, such as for $\Gamma_1 = \Gamma_2 = -\Gamma_3$ in Fig. 2b, separatrices are also given by level curves passing through the phase space point corresponding to the equilateral triangle configuration. The primary distinctions between different regimes of motion are whether or not the configuration ever becomes colinear and if the relative vortex spacing remains finite.

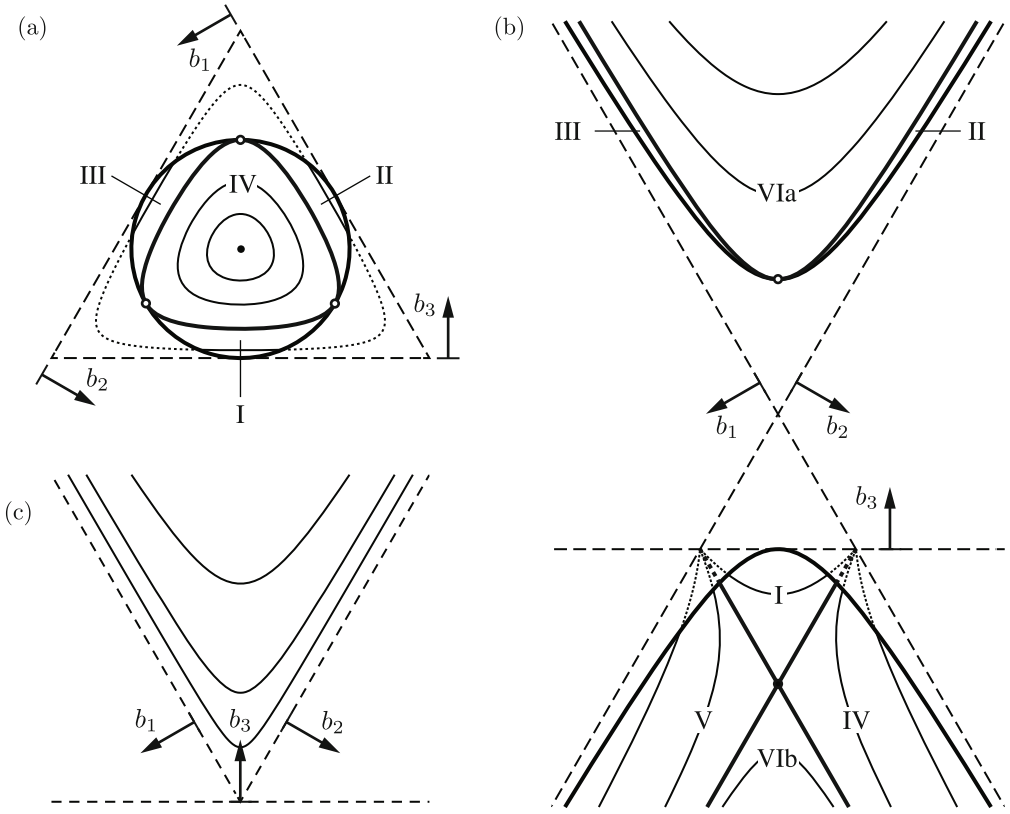


**Fig. 2.** Phase space representations in the $(b_1, b_2, b_3)$ plane for (a) $\Gamma_1 = \Gamma_2 = \Gamma_3$ or $G_1 = G_2 = G_3 = 1$ and for (b), (c) $\Gamma_1 = \Gamma_2 = -\Gamma_3$ or $G_1 = G_2 = -G_3 = 1$ with (b) $L \neq 0$ and (c) $L = 0$. Solid and open circles mark the equilateral triangle and colinear equilibria, respectively. Level curves of (a), (b) Eq. (2.7) and (c) Eq. (2.10) are shown with light solid lines in the physical regions; dotted lines denote inaccessible regions. Heavy solid lines show the boundaries of the physical regions and the separatrices. Regimes of motion are labeled with Roman numerals to match the definitions in Section 4.

## 3. PROBLEM FORMULATION

In an alternative approach, the vortex configuration can be represented in terms of the interior angles of the triangle, $\theta_j$ $(j = 1, 2, 3)$, the radius of the circle circumscribed on that triangle, $R$, the location of the center of that circumcircle, $Z = X + \mathrm{i}\, Y$, and the orientation of the triangle as determined by one of the vortex angles, $\phi_j$, as illustrated in Fig. 1. A derivation of the equations of motion in terms of these variables can be found in Ref. [12], and in Ref. [13] this formulation is used for a detailed analysis of self-similar collapse and expansion. It is shown below that, similar to the classic analysis in Section 2, this formulation also enables characterization of the relative vortex motion in a phase space described by trilinear coordinates.

### *3.1. Trilinear Coordinates*

The absolute vortex locations can be given by

$$z_j = Z + Re^{\mathrm{i}\phi_j}, \quad j = 1, 2, 3. \tag{3.1}$$

Assume without any loss of generality that the vortices are initially labeled counterclockwise as shown in Fig. 1a. In this case, the interior angles $\theta_k$ are related to the vortex angles $\phi_j$ as

$$2\theta_1 = \phi_3 - \phi_2, \quad 2\theta_2 = 2\pi + (\phi_1 - \phi_3), \quad 2\theta_3 = \phi_2 - \phi_1. \tag{3.2a}$$

Suppose the subsequent vortex motion has vortex 1 passing between vortices 2 and 3, as illustrated in Fig. 1b. Without relabeling the vortices and maintaining a smooth transition in the angles, this motion produces a clockwise orientation of the vortices and the labeling of $\theta_j$ as shown in Fig. 1c, for which the angle relationships are

$$2\theta_1 = 2\pi + (\phi_3 - \phi_2), \quad 2\theta_2 = \phi_1 - \phi_3, \quad 2\theta_3 = \phi_2 - \phi_1. \tag{3.2b}$$

Alternatively, vortex 2 may pass between vortices 1 and 3, or vortex 3 between 1 and 2; each of these motions produces angle relationships like those in (3.2), with an additive term of $2\pi$ appearing in various terms. Furthermore, as the vortices evolve the angles $\phi_j$ may increment by multiples of $2\pi$. In general, for any three-vortex configuration evolving from an initial counterclockwise configuration, the relationships between the triangle angles $\theta_k$ and the vortex angles $\phi_j$ can be written as

$$2\theta_1 = 2\pi n_1 + (\phi_3 - \phi_2), \quad 2\theta_2 = 2\pi n_2 + (\phi_1 - \phi_3), \quad 2\theta_3 = 2\pi n_3 + (\phi_2 - \phi_1), \tag{3.3}$$

where the $n_j$ are integers. The triangle lengths (2.1) used in the classic formulation are given by

$$s_j = 2R\,|\sin\theta_j|\,, \quad j = 1, 2, 3. \tag{3.4}$$

By the triangle angle theorem, it is required that

$$\theta_1 + \theta_2 + \theta_3 = \pi \tag{3.5}$$

for any of the allowed labelings. Analogous to the classic triangle formulation, the motion can be represented in phase space using trilinear coordinates, which in this case is the $(\theta_1, \theta_2, \theta_3)$-plane. In contrast to the classic formulation summarized in Section 2, the fundamental equation for these trilinear coordinates (3.5) is exactly the constraint that the vortex configuration be a triangle, and thus in the present formulation there does not exist a parameter-dependent phase plane boundary such as given by (2.6).

A representation of the $(\theta_1, \theta_2, \theta_3)$-plane is shown in Fig. 3. The triangular region in which $0 \leqslant \theta_1, \theta_2, \theta_3 \leqslant \pi$ will be referred to as the *fundamental region*; by geometric similarity, all other physically accessible regions in the phase plane are identical to this fundamental region through reflection and/or translation. With the assumption that the initial vortex configuration is labeled as shown in Fig. 1a, all initial conditions are located in this fundamental region. Each of the vertices where two axes (or their periodic images) intersect, for which $\theta_j = \pi n_j$ with $n_j$ an integer, corresponds to a colinear configuration. As the vortex configuration passes through a colinear configuration, the level curve in phase space passes through a vertex from one triangular region to the next, as illustrated in Fig. 3 for the transition depicted in Fig. 1.

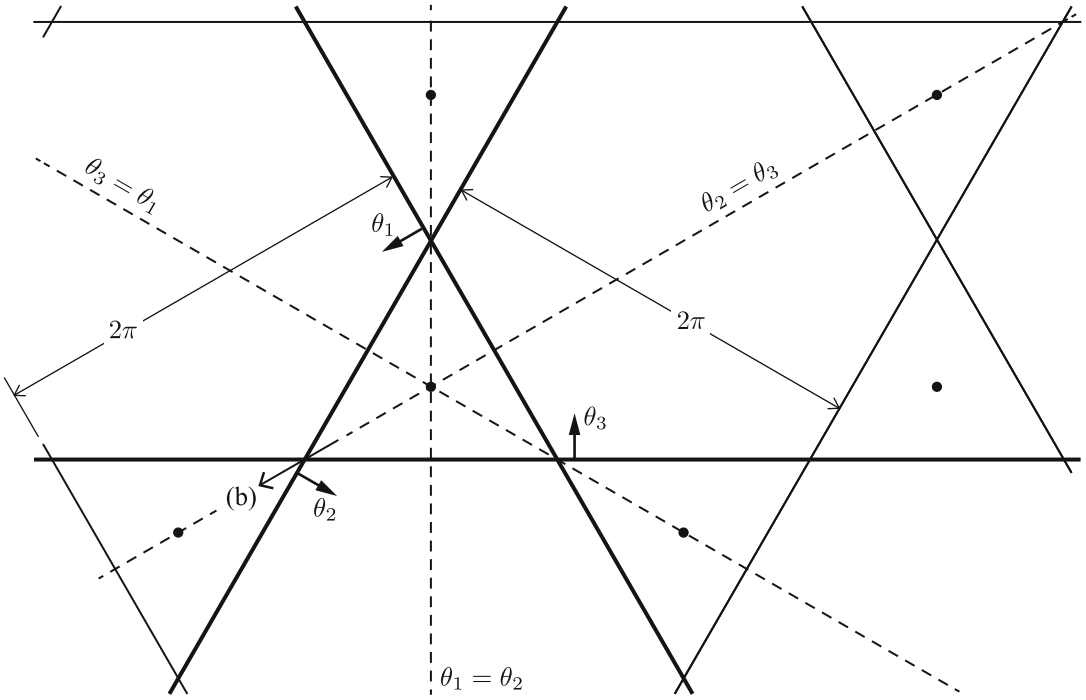


**Fig. 3.** Phase space representation in a portion of the periodic $(\theta_1, \theta_2, \theta_3)$ plane. The $\theta_j$ axes are shown with heavy solid lines, and $2\pi$-periodic images of these axes are shown with light solid lines. Vertices at the intersections of solid lines correspond to colinear configurations. The full phase space consists only of the triangular regions, which surround inaccessible hexagonal regions. Passing through a colinear configuration corresponds to moving from one triangular region to the next; the arrow labeled (b) represents the transition illustrated in Fig. 1b. Adjacent triangular regions are related through reflective symmetry. Solid circles mark the equilateral triangle configuration that is always in relative equilibrium. Dashed lines show axes of symmetry in the system that correspond to interchanging two of the vortex labels.

### *3.2. Constants of Motion*

Similar to the classic analysis, the relative vortex motion can be characterized by considering level curves of the Hamiltonian in the phase plane, which here is the $(\theta_1, \theta_2, \theta_3)$-plane instead of the $(b_1, b_2, b_3)$-plane. By substituting (3.4) into (1.8) and (1.10), respectively, and using the notation introduced in (1.2)–(1.3), these constants of the motion can be written in normalized form as

$$\tilde{L} = \frac{L}{4\Gamma_0^2 R_0^2} = \frac{\gamma_3 R^2}{\Gamma_0^2 R_0^2} \sum_{j=1}^{3} \frac{\sin^2\theta_j}{\Gamma_j} = \frac{\rho^2}{g_3} \sum_{j=1}^{3} G_j \sin^2\theta_j \tag{3.6}$$

and

$$\tilde{H} = \frac{4\pi\,(H + H_0)}{\Gamma_0^2} = -\frac{\gamma_2}{\Gamma_0^2} \ln\left(\frac{R}{R_0}\right)^2 - \frac{\gamma_3}{\Gamma_0^2} \sum_{j=1}^{3} \frac{\ln\left(\sin^2\theta_j\right)}{\Gamma_j} = -\frac{g_1}{g_3} \ln\rho^2 - \frac{1}{g_3} \sum_{j=1}^{3} G_j \ln\left(\sin^2\theta_j\right), \tag{3.7}$$

where $\rho = R/R_0$ is the circle radius normalized by the initial radius, $R_0$, and $H_0 = \frac{1}{2\pi}\,\gamma_2 \ln(2R_0)$.

It has been known since Gröbli's analysis [6, 10] that the special case $\tilde{L} = 0$, $g_1 = 0$ corresponds to self-similar motion of the vortex triangle for which the interior angles $\theta_j$ are each constant in time, and numerous authors have investigated this problem; see, for example, [1, 11, 14, 17, 18]. If $\tilde{L} = 0$, then Eq. (3.6) reduces to

$$\sum_{j=1}^{3} G_j \sin^2\theta_j = 0, \tag{3.8}$$

independent of $\rho$. Equation (3.8) has solutions only when the configuration contains vortices of opposite sign. If $g_1 = 0$, which also requires vortices of opposite sign, then $\tilde{H}$ is also independent of $\rho$, and Eq. (3.7) can be written as

$$f_0(\theta_1, \theta_2, \theta_3; G_1, G_2, G_3) = \prod_{j=1}^{3} \left(\sin^2 \theta_j\right)^{G_j} = \exp\left(-g_3 \tilde{H}\right) \equiv \mathbb{C}_0, \tag{3.9}$$

with $\mathbb{C}_0 =$ constant during the motion. For specified values of $G_j$ satisfying $g_1 = 0$, the three Eqs. (3.5), (3.9), and (3.8) can be viewed as defining three surfaces in $(\theta_1, \theta_2, \theta_3)$-space that intersect at most at isolated points, so that taking both $g_1 = 0$ and $\tilde{L} = 0$ allows only for solutions with constant internal angles. Alternatively, for this special case one can consider (3.8) as determining all triangle configurations that produce self-similar motion for specified strength ratios; similarly, substituting (3.8) and $g_1 = 0$ into (3.9) determines those configurations that produce self-similar motion for specified values of the Hamiltonian. For further details regarding self-similar expansion or collapse using a formulation in $(\theta_1, \theta_2, \theta_3)$-space, the reader is referred to Ref. [13].

If $g_1 = 0$ with $\tilde{L} \neq 0$, the evolution of the vortex triangle lies on level curves of (3.9) in the phase space defined by the trilinear coordinates $(\theta_1, \theta_2, \theta_3)$. In this case, the dimensionless radius of the circumcircle, $\rho$, evolves in time so as to satisfy the constraint of Eq. (3.8).

If $g_1 \neq 0$ (equivalently, $\gamma_2 \neq 0$), a phase space representation is obtained for $\tilde{L} \neq 0$ by combining Eqs. (3.6) and (3.7) to eliminate $\rho$, giving

$$f(\theta_1, \theta_2, \theta_3; G_1, G_2, G_3) = \frac{\prod_{j=1}^{3} \left(\sin^2 \theta_j\right)^{G_j}}{\left(\sum_{k=1}^{3} G_k \sin^2 \theta_k\right)^{g_1}} = \frac{\exp\left(-g_3 \tilde{H}\right)}{\left(g_3 \tilde{L}\right)^{g_1}} \equiv \mathbb{C}, \tag{3.10}$$

with $\mathbb{C}$ a constant that specifies which level curve is being considered in $(\theta_1, \theta_2, \theta_3)$-space. Although derived separately, taking $g_1 = 0$ in (3.10) yields (3.9).

If instead $\tilde{L} = 0$ with $g_1 \neq 0$, Eq. (3.8) can be used to determine the corresponding level curves in phase space, with (3.7) subsequently giving the circumcircle radius.

### *3.3. Characterizing the Fixed Point $\theta_1 = \theta_2 = \theta_3 = \pi/3$*

As noted in Section 1, the equilateral triangle configuration with $\theta_1 = \theta_2 = \theta_3 = \pi/3$ is a relative equilibrium configuration independent of the circumcircle radius, the vortex strengths, and the triangle orientation, so that $(\theta_1, \theta_2, \theta_3) = \frac{1}{3}(\pi, \pi, \pi) \equiv \boldsymbol{\theta}_e$ (or any of the periodic images) is a fixed point in phase space for every case. The topological structure of the level curves in phase space, as given by (3.9) or (3.10), depends on whether this fixed point is a (neutral) center point or a saddle point. Assuming $g_1 \neq 0$, first combine (3.5) and (3.10) to eliminate one of the triangle angles from the analysis. By eliminating $\theta_1 = \pi - \theta_2 - \theta_3$, for example, the function in (3.10) can be written as

$$f(\pi - \theta_2 - \theta_3, \theta_2, \theta_3) = \frac{\left(\sin(\theta_2 + \theta_3)\right)^{2G_1} \left(\sin\theta_2\right)^{2G_2} \left(\sin\theta_3\right)^{2G_3}}{\left[G_1 \sin^2(\theta_2 + \theta_3) + G_2 \sin^2\theta_2 + G_3 \sin^2\theta_3\right]^{g_1}}, \tag{3.11}$$

with the value of the constant for this relative equilibrium configuration being

$$\mathbb{C}' \equiv f(\pi/3, \pi/3, \pi/3) = g_1^{-g_1}. \tag{3.12}$$

From applying the second derivative test to Eq. (3.11), the sign of the discriminant at the fixed point

$$D \equiv \left[\frac{\partial^2 f}{\partial\theta_2^2}\frac{\partial^2 f}{\partial\theta_3^2} - \left(\frac{\partial^2 f}{\partial\theta_2\,\partial\theta_3}\right)^2\right]_{\theta_j = \pi/3} = \frac{16\, g_3}{g_1^{1+2g_1}} \tag{3.13}$$

classifies this point as a center (for $D > 0$) or a saddle (for $D < 0$). The fixed point classification is thus determined fully by

$$\delta \equiv \frac{g_3}{g_1} = \frac{G_1 G_2 G_3}{G_1 + G_2 + G_3} = \frac{\Gamma_0^2}{\gamma_2} = \frac{\Gamma_0^2}{\Gamma_1\Gamma_2 + \Gamma_2\Gamma_3 + \Gamma_3\Gamma_1}, \tag{3.14}$$

since $\mathrm{sign}(D) = \mathrm{sign}(\delta)$. If $\delta > 0$ the fixed point $\boldsymbol{\theta}_e$ is a (neutral) center, and if $\delta < 0$ it is a saddle point. The transitions between these types occur when $\delta = 0$ or $\delta \to \infty$. Without any loss of generality, assume that $\Gamma_0 = \Gamma_1$, so that $G_1 = 1$. Fixed point behavior can then be classified in $(G_2, G_3)$-parameter space, with changes in classification delineated by $G_2 = 0$, $G_3 = 0$, and $G_3 = -(G_2 + 1)$, as illustrated in Fig. 4. As $G_3 \to -(G_2 + 1)$, $D \to \pm\infty$, and this line corresponds to the case $g_1 = \gamma_2 = 0$, for which the fixed point at $\theta_1 = \theta_2 = \theta_3 = \pi/3$ is degenerate.

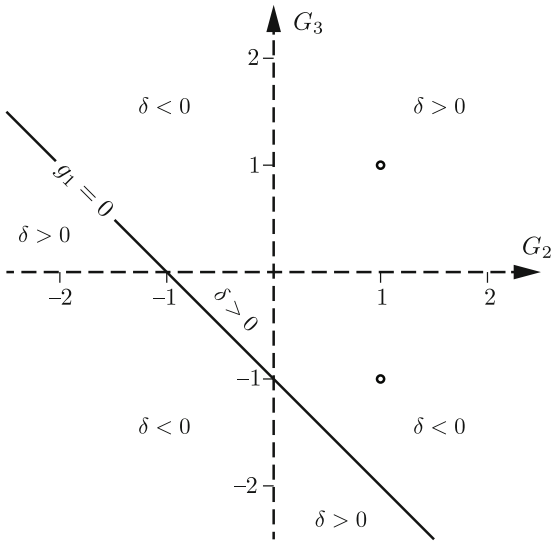


**Fig. 4.** Parameter space in the vortex strength ratios with the assumption that $G_1 = 1$. Dashed lines (the axes) are not allowed by the assumption that $\Gamma_j \neq 0$. The solid line is the special case $g_1 = 0$ (or $\gamma_2 = 0$). Regions are distinguished by the sign of $\delta$ (3.14). Open circles mark the examples discussed in Section 4.

### *3.4. Colinear Configurations*

When viewed from the perspective of phase space, the colinear configurations that rotate and/or translate uniformly as relative equilibria and the corresponding triangle configurations that asymptotically approach these relative equilibrium states delineate between those triangle configurations that periodically pass through a colinear state and those that evolve without the vortices ever becoming colinear. In the classic approach, the colinear relative equilibria correspond to phase space points at which the level curves of (2.7) or (2.10) are tangent to the boundaries of the physical regions defined by (2.6), and for $\delta > 0$ those level curves delineate distinct regions in phase space [1]. In the present formulation, all colinear configurations, including both transient and (relative) equilibrium states, correspond to the intersections of axes in phase space where $\theta_j = \pi n_j$ (for integers $n_j$). These points are degenerate, with $\rho \to \infty$ and $\sin\theta_j \to 0$ simultaneously in the equations for $\tilde{L}$ (3.6) and $\tilde{H}$ (3.7), and with a continuum of relevant phase space level curves accumulating at each point. The definitions of $f_0(\theta_j; G_j) = \mathbb{C}_0$ (3.9) and $f(\theta_j; G_j) = \mathbb{C}$ (3.10), however, are independent of $\rho$, so that the unique level curves connecting colinear relative equilibria are well defined. Determining the corresponding values of $\mathbb{C}$ (or $\mathbb{C}_0 = \mathbb{C}|_{g_1=0}$) is best accomplished by solving directly for these equilibrium states. Detailed studies of colinear three-point-vortex equilibria have been conducted by several authors, including Refs. [5, 7, 11]; the brief discussion here will follow most closely the analysis by Aref [5].

When the vortex configuration is moving in relative equilibrium as a rigid body, the velocity of every vortex consists of a translation and a rotation, so that the equations of motion (1.4) become

$$\overline{V + \mathrm{i}\Omega z_j} = \frac{1}{2\pi\mathrm{i}} \sum_{\substack{k=1 \\ k\neq j}}^{3} \frac{\Gamma_k}{z_j - z_k}, \tag{3.15}$$

where $V$ is generally complex-valued and $\Omega$ is real. Multiplying (3.15) by $\Gamma_k$ and summing shows that

$$\gamma_1 V + \mathrm{i}\Omega\, Q = 0. \tag{3.16}$$

Multiplying (3.15) instead by $\Gamma_k z_k$ and summing gives

$$V\overline{Q} + \mathrm{i}\Omega\, I = -\frac{\gamma_2}{2\pi\mathrm{i}}. \tag{3.17}$$

Any colinear configuration can be assumed to lie instantaneously on the $x$ axis, in which case (3.15) can be written as

$$a + bx_1 = \frac{\Gamma_2\xi_2 - \Gamma_3\xi_3}{\xi_2\xi_3}, \quad a + bx_2 = \frac{\Gamma_3\xi_3 - \Gamma_1\xi_1}{\xi_3\xi_1}, \quad a + bx_3 = \frac{\Gamma_1\xi_1 - \Gamma_2\xi_2}{\xi_1\xi_2}, \tag{3.18}$$

where $a = 2\pi\mathrm{i}\overline{V}$, $b = 2\pi\Omega$, and

$$\xi_1 = x_2 - x_3, \quad \xi_2 = x_3 - x_1, \quad \xi_3 = x_1 - x_2, \tag{3.19}$$

with

$$\xi_1 + \xi_2 + \xi_3 = 0. \tag{3.20}$$

Equations (3.18) are all real-valued, so that at this instant $V$ must be purely imaginary. If $b = 0$ and $a \neq 0$, then (3.16) requires that $\gamma_1 = 0$. However, translating equilibrium solutions do not exist for this balance of strengths when there are only three vortices; see Ref. [5] for a proof. If $b \neq 0$, the origin can be chosen so that $a = 0$ in (3.18), and then $Q = 0$ by (3.16). Hence, there are two situations to consider: the configuration is completely stationary with $V = \Omega = 0$ or the configuration rotates rigidly with $\Omega \neq 0$ and $V = Q = 0$.

Consider the general case of relative equilibria with $V = 0$ and $\Omega \neq 0$. Multiplying each of the equations in (3.18) by $\xi_j^{-1}$ and summing gives (for $a = 0$, $b \neq 0$)

$$\frac{x_1}{\xi_1} + \frac{x_2}{\xi_2} + \frac{x_3}{\xi_3} = 0. \tag{3.21}$$

Combining $Q = 0$ with Eqs. (3.19) gives

$$\Gamma_2\xi_3 - \Gamma_3\xi_2 = \gamma_1 x_1, \quad \Gamma_3\xi_1 - \Gamma_1\xi_3 = \gamma_1 x_2, \quad \Gamma_1\xi_2 - \Gamma_2\xi_1 = \gamma_1 x_3. \tag{3.22}$$

For $\gamma_1 \neq 0$ (i. e., $g_2 \neq 0$), Eqs. (1.2) and (3.22) can then be substituted into (3.21) to give

$$\frac{1}{G_1\, G_2}\left(\frac{\xi_1}{\xi_2} - \frac{\xi_2}{\xi_1}\right) + \frac{1}{G_2\, G_3}\left(\frac{\xi_2}{\xi_3} - \frac{\xi_3}{\xi_2}\right) + \frac{1}{G_3\, G_1}\left(\frac{\xi_3}{\xi_1} - \frac{\xi_1}{\xi_3}\right) = 0. \tag{3.23}$$

Defining the vortex separation ratio as

$$\zeta \equiv \frac{\xi_1}{\xi_3}, \quad \frac{\xi_2}{\xi_3} = -(1+\zeta), \quad \frac{\xi_2}{\xi_1} = -\left(1 + \frac{1}{\zeta}\right), \tag{3.24}$$

Eq. (3.23) becomes the polynomial [5, 7, 11]

$$p(\zeta) = G_3(G_1 + G_2)\,\zeta^3 + G_3(G_1 + 2G_2)\,\zeta^2 - G_1(2G_1 + G_3)\,\zeta - G_1(G_2 + G_3) = 0, \tag{3.25}$$

which will always have at least one real root, denoted $\zeta_j^*$. The values $\zeta = 0, -1$ correspond to singular cases in which two vortices occupy the same point, so solutions $\zeta_j^* \neq 0, -1$ define the colinear relative equilibrium configurations for $b \neq 0$, $\gamma_1 \neq 0$ (or $g_2 \neq 0$).

These colinear equilibrium configurations correspond to unique values of the constant in Eq. (3.10). In the limit of a colinear configuration, combining the original definitions of $L$ (1.8) and $H$ (1.10) with $z_j - z_k \to x_j - x_k$ and the nondimensionalization in (3.6) and (3.7) gives

$$\frac{\exp\left(-g_3\,\tilde{H}\right)}{\left(g_3\,\tilde{L}\right)^{g_1}} \to \frac{\xi_1^{2G_1}\,\xi_2^{2G_2}\,\xi_3^{2G_3}}{\left(G_1\xi_1^2+G_2\xi_2^2+G_3\xi_3^2\right)^{g_1}} = \frac{\left(\xi_2/\xi_1\right)^{2G_2}\left(\xi_3/\xi_1\right)^{2G_3}}{\left(G_1+G_2\left(\xi_2/\xi_1\right)^2+G_3\left(\xi_3/\xi_1\right)^2\right)^{g_1}}. \tag{3.26}$$

By substitution of (3.24) into (3.26), the relative equilibrium configurations given by $\zeta_j^*$ define the corresponding constants

$$\mathbb{C}_j^* \equiv \frac{\left(\zeta_j^*\right)^{2G_1}\left(\zeta_j^*+1\right)^{2G_2}}{\left(G_1\left(\zeta_j^*\right)^2+G_2\left(\zeta_j^*+1\right)^2+G_3\right)^{g_1}}; \tag{3.27}$$

this includes the cases with $g_1 = 0$.

If $\gamma_1 = g_2 = 0$ (with $a = 0$, $b \neq 0$), then Eq. (3.22) gives

$$\frac{\xi_1}{\Gamma_1} = \frac{\xi_2}{\Gamma_2} = \frac{\xi_3}{\Gamma_3} \equiv \Xi, \tag{3.28}$$

which can be substituted into Eq. (3.18) to give the vortex positions producing a relative equilibrium configuration,

$$x_1^* = \frac{\Xi}{b}\left(\frac{\Gamma_3}{\Gamma_2}-\frac{\Gamma_2}{\Gamma_3}\right), \quad x_2^* = \frac{\Xi}{b}\left(\frac{\Gamma_1}{\Gamma_3}-\frac{\Gamma_3}{\Gamma_1}\right), \quad x_3^* = \frac{\Xi}{b}\left(\frac{\Gamma_2}{\Gamma_1}-\frac{\Gamma_1}{\Gamma_2}\right), \tag{3.29}$$

where $\Xi/b$ can be considered an arbitrary scale factor. Note that with $\gamma_1 = 0$ and $Q\ (+\mathrm{i}P) = 0$, Eq. (1.8) gives $L = 0$. In this case the isolated level curves in phase space are already given by Eq. (3.8), and the colinear equilibria do not provide any additional phase space information.

## 4. TWO CANONICAL EXAMPLES

To illustrate the use of this alternative formulation in categorizing and comparing the relative motion of three vortices on the plane, consider the canonical cases with $\Gamma_1 = \Gamma_2 = \pm\Gamma_3$. For each of these examples it is assumed without any loss of generality that $\Gamma_0 = \Gamma_1$, so that $G_1 = 1$ and $(G_2, G_3) = (1, \pm 1)$. Comparisons of these examples with previous results from the literature [1, 3, 6, 7, 10, 15, 16, 18] help illustrate the role that this alternative formulation can play in understanding the vortex motion.

The general investigative procedure is as follows. For given values of $G_2$, $G_3$ with $g_1 \neq 0$, use (3.10) to determine level curves in phase space. The topological structure of phase space is determined by the sign of $\delta$ (3.14). If $\delta > 0$, the colinear relative equilibria give level curves, or separatrices, that divide phase space into different regimes of motion. If instead $\delta < 0$, separatrices are also given by the level curves emanating from the saddle point at $\theta_j = \pi/3$. Real-space vortex trajectories corresponding to a phase space level curve are determined by direct integration of (1.4). In all cases shown here, integration times have been normalized by the characteristic time $T = R_0^2/\Gamma_0$, with $\hat{t} = t/T$ being the dimensionless time, and initial positions have been chosen so that $\phi_1(\hat{t}) = 0$ for $\hat{t} = 0$. The relative vortex motions within any given regime of motion are qualitatively similar, and thus it is necessary to consider only one representative example from each regime.

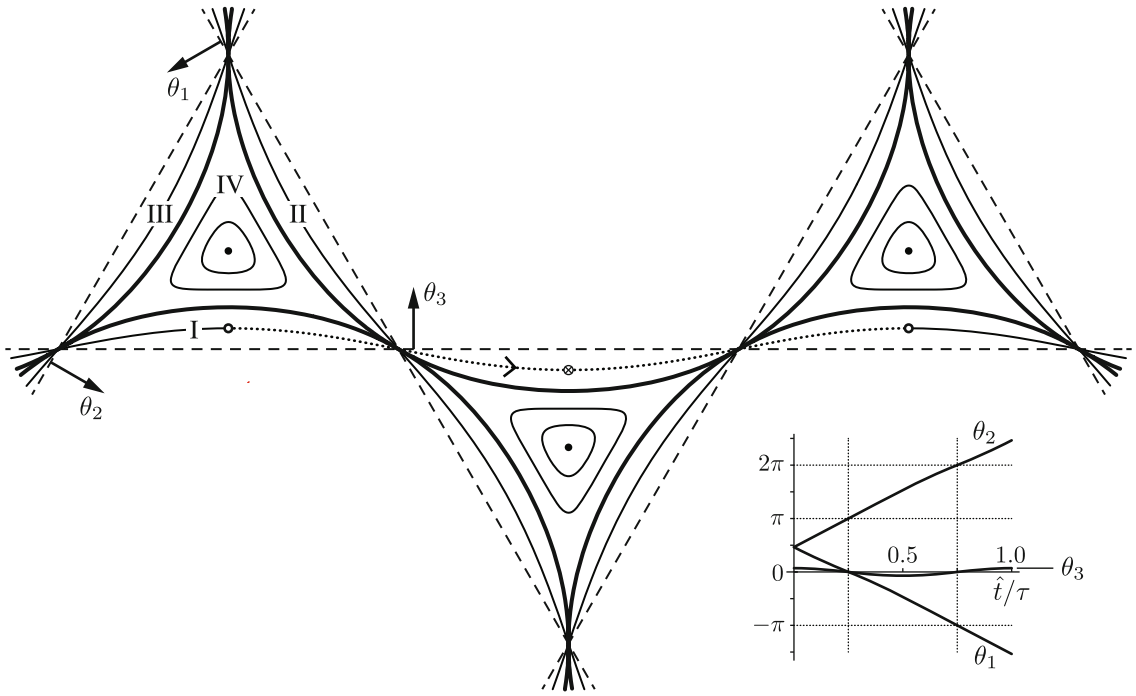


**Fig. 5.** Representative level curves in the $(\theta_1, \theta_2, \theta_3)$ phase space for $G_1 = G_2 = G_3 = 1$ $(\Gamma_1 = \Gamma_2 = \Gamma_3)$. Heavy solid lines are the separatrices given by (4.1) for $\mathbb{C}^* = 1/54$; light solid lines are level curves for $\mathbb{C} = \{1/175, 1/35, 1/29\}$. The dotted line shows one period of the phase-space trajectory for the real-space motion shown in Fig. 6; open circles mark the initial and final positions, $\otimes$ marks the half-period position, and the arrow indicates the direction of motion. Solid circles mark the equilateral triangle relative equilibrium configuration (*inset, lower right*). Variation in the angles $\theta_j$ as a function of time for the example trajectory; vertical lines indicate where the configuration becomes colinear.

### *4.1. The Case $G_1 = G_2 = G_3 = 1$ $(\Gamma_1 = \Gamma_2 = \Gamma_3)$*

A commonly considered case of three-vortex motion comes from taking $\Gamma_1 = \Gamma_2 = \Gamma_3$, so that $G_1 = G_2 = G_3 = 1$. With this choice of strengths, the symmetric functions in (1.1a) and (1.3) give $\gamma_1 = \gamma_2 = g_1 = g_2 = 3$ and $\gamma_3 = g_3 = 1$. A representation of the $(\theta_1, \theta_2, \theta_3)$ phase space in this case is shown in Fig. 5; the corresponding representation in $(b_1, b_2, b_3)$ phase space is given in Fig. 2a. Since $G_j > 0$, by (3.6) it is clear that $\tilde{L} \neq 0$ for any noncolinear configuration. By (3.10), the level curves are given by

$$\mathbb{C} = \frac{\left(\sin^2\theta_1\right)\left(\sin^2\theta_2\right)\left(\sin^2\theta_3\right)}{\left(\sin^2\theta_1 + \sin^2\theta_2 + \sin^2\theta_3\right)^3}. \tag{4.1}$$

By (3.14), $\delta = 1/3 > 0$, so that the point in phase space given by the equilateral triangle configuration is a center. Illustrated in Fig. 5 are the fundamental triangular region, for which $0 \leqslant \theta_1, \theta_2, \theta_3 \leqslant \pi$, and two of the image regions: the region given by $-\pi \leqslant \theta_1, \theta_3 \leqslant 0$ and $\pi \leqslant \theta_2 \leqslant 2\pi$ is a rotation of the fundamental region about the point $\theta_1 = \theta_3 = 0$, and the region given by $-2\pi \leqslant \theta_1 \leqslant -\pi$, $2\pi \leqslant \theta_2 \leqslant 3\pi$, and $0 \leqslant \theta_3 \leqslant \pi$ is a translation of the fundamental region. Since the vortices are indistinguishable, the phase space representation is symmetric about each of the lines $\theta_1 = \theta_2$, $\theta_2 = \theta_3$, and $\theta_3 = \theta_1$.

For this set of strengths, the solutions of $p(\zeta) = 0$ (3.25) are $\{\zeta_1^*, \zeta_2^*, \zeta_3^*\} = \{-2, -1/2, 1\}$, which all correspond to the same colinear (unstable) relative equilibrium configuration: three identical vortices equally spaced on a line. By (3.27), this gives $\mathbb{C}_1^* = \mathbb{C}_2^* = \mathbb{C}_3^* = 1/54 \equiv \mathbb{C}^*$. As shown in Fig. 5, the level curves given by $\mathbb{C} = \mathbb{C}^* = 1/54$ connect each of the vertices formed by the $\theta_j$ axes and separate the fundamental region into four *regimes of motion*, labeled I–IV: regimes I–III in which all level curves connect two phase space vertices, and regime IV containing closed curves that encircle the equilateral triangle equilibrium point and do not intersect the phase space vertices. By symmetry, regimes I–III are identical except for a relabeling of the vortices.

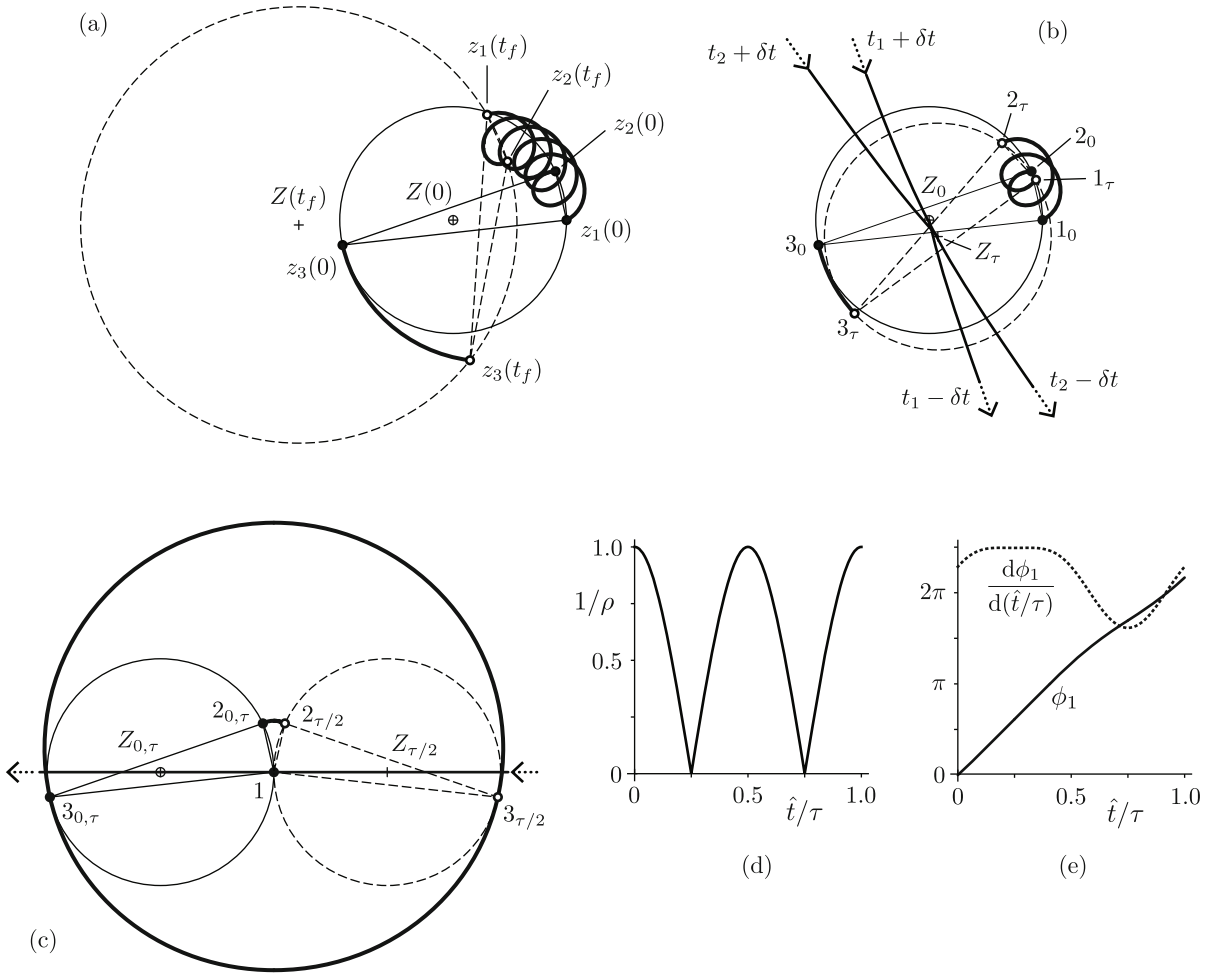


**Fig. 6.** Example real-space vortex trajectories in the $(x, y)$ plane for $G_1 = G_2 = G_3 = 1$, $\mathbb{C} = 1/175$, and initial angles $\theta_3 \approx 0.222$, $\theta_1 = \theta_2 = \frac{1}{2}(\pi - \theta_3)$, corresponding to the phase space point identified in Fig. 5. (a) *Orbiting* vortex trajectories (heavy solid lines) in a fixed frame of reference for an arbitrary duration $\hat{t}_f = 10$. Initial vortex positions are marked by solid circles, and final positions are marked by open circles. Initial and final positions of the circumcenter are marked with the symbols $\oplus$ and $+$, respectively. Initial and final positions of the triangle and circumscribed circle are shown with solid lines and dashed lines, respectively. (b) Vortex trajectories in a fixed frame for one temporal period of the relative motion, $0 \leqslant \hat{t} \leqslant \tau \approx 4.27$. Also shown is the trajectory of the circumcenter $Z(\hat{t})$; arrows show the direction of motion, and dotted lines indicate progression to/from infinity. Vortex positions $z_j(\hat{t})$ are labeled according to the index $j$, with subscript indicating the corresponding time $\hat{t}$; the circumcenter position is labeled with the notation $Z_{\hat{t}} \equiv Z(\hat{t})$. (c) Vortex and circumcenter trajectories in the moving frame defined by Eq. (4.3) with vortex 1 as the reference. Positions at times $\hat{t} = n\tau$, $n = 0, 1, \ldots$, which are identical for vortices, triangle, circumcircle, and circumcenter, are shown with solid circles, solid lines, and $\oplus$, respectively; positions at the half-periods, $\hat{t} = (2n+1)\tau/2$, $n = 0, 1, \ldots$, are shown with open circles, dashed lines, and $+$. Vortex 1 remains stationary in this frame. (d), (e) Corresponding evolution for one temporal period of (d) the radius of the circumcircle, shown as $1/\rho = R_0/R$ to clearly represent the colinear states for which $R \to \infty$, and (e) the (rate of change of) orientation of the triangle in a fixed frame, as given by (the temporal derivative of) $\phi_1(t)$.

Consider first motions from regime I. The representative level curve in this regime shown in Fig. 5 is given by $\mathbb{C} = 1/175$, and the initial condition marked by the open circle is an isosceles triangle configuration with $\theta_1 = \theta_2 = (\pi - \theta_3)/2$. The real-space motion is shown in Fig. 6a for an arbitrary length of time, $0 \leqslant \hat{t} \leqslant \hat{t}_f = 10$. The relative vortex positions, represented by the vortex triangle, repeat periodically in time with a period $\tau \approx 4.27$, as shown in Fig. 6b; this time period was determined numerically by monitoring the value of the angle $\theta_1$. The corresponding phase space trajectory for one period of motion is shown in Fig. 5 by the dotted line, with the

open circles marking identical isosceles triangle configurations that differ only by values of $2\pi n_j$ in the definitions of the angles $\theta_j$. This example illustrates that the phase space trajectory can be represented fully by showing level curves in just the fundamental region.

In a fixed frame of reference, the net motion consists of the closely-spaced vortices 1 and 2 orbiting as a pair and vortex 3 moving relatively slowly at a distance. With each period of relative motion there is a translation and rotation of the vortex triangle. The orientation of the vortex triangle can be quantified by any one of the angles $\phi_j$; the variation of $\phi_1$ and its temporal rate of change over one period $\tau$ is shown in Fig. 6e. The configuration becomes colinear twice during each period of motion; for this choice of initial condition, colinearity occurs (during the first period) at $\hat{t}_1 = \tau/4$ and $\hat{t}_2 = 3\tau/4$. The radius of the circumscribed circle becomes infinite when the configuration becomes colinear, as shown in Fig. 6d. The positions of the vortices and the corresponding triangle remain finite, and passing through the colinear arrangement reorients the circumcircle, so in these cases the location of the circumcenter "passes through" (complex) infinity, as illustrated in Fig. 6b. All initial conditions from regime I produce qualitatively similar orbiting motion.

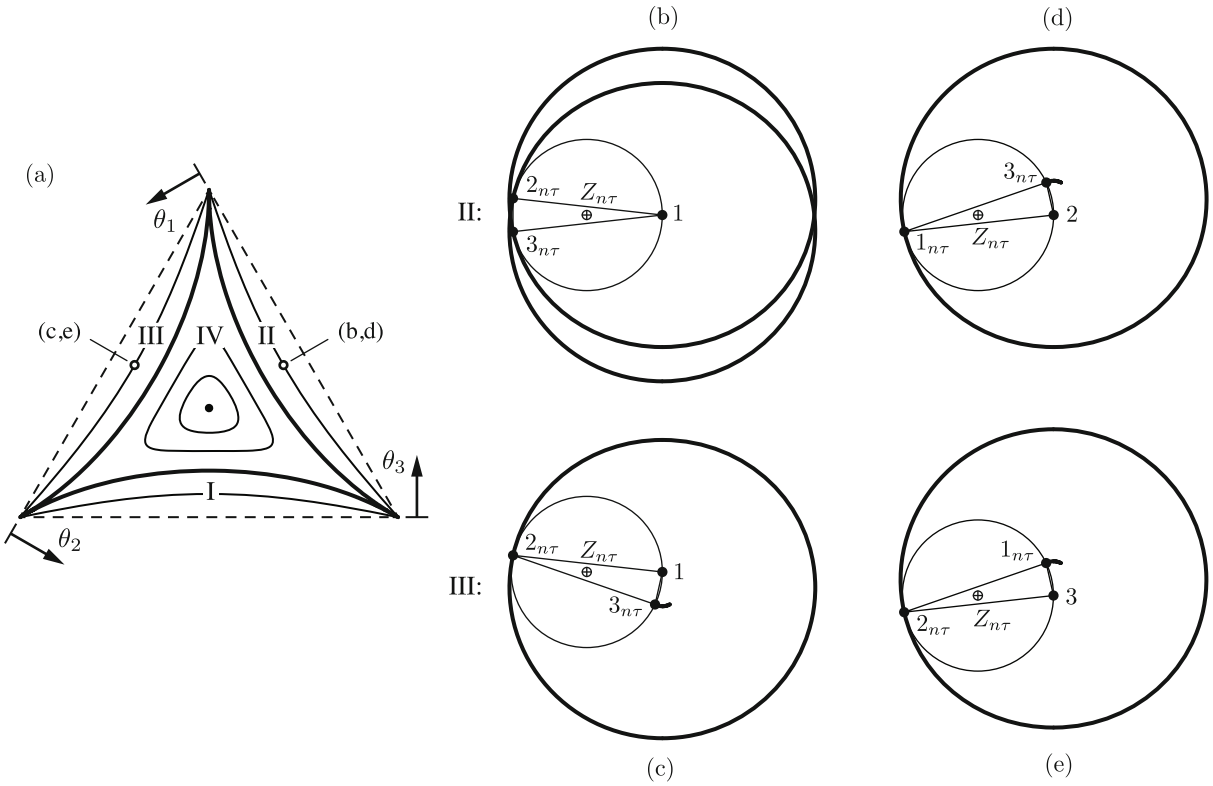


**Fig. 7.** Representative vortex trajectories from regimes II and III for $G_1 = G_2 = G_3 = 1$. (a) The phase space representation, with initial positions marked by open circles on the level curve given by $\mathbb{C} = 1/175$. (b)–(e) *Orbiting* vortex trajectories (heavy lines) in a co-moving frame of reference; initial vortex positions and periodic images are shown with solid circles, initial triangle and circumcircle are shown with light lines, and the initial position and periodic images of the circumcenter are located at $\oplus$. Positions of the circumcenter and the moving vortices are labeled $j_{n\tau}$ and $Z_{n\tau}$, respectively, indicating that these are the positions at times $\hat{t} = n\tau$, $n = 0, 1, 2, \ldots$; the vortex stationary in the chosen frame is labeled with no subscript. (b), (d) Co-moving trajectories for the initial condition $\theta_1 \approx 0.222$, $\theta_2 = \theta_3 = \frac{1}{2}(\pi - \theta_1)$ in regime II with (b) vortex 1 as reference and (d) vortex 2 as reference. (c), (e) Co-moving trajectories for the initial condition $\theta_2 \approx 0.222$, $\theta_1 = \theta_3 = \frac{1}{2}(\pi - \theta_2)$ in regime III with (c) vortex 1 as reference and (e) vortex 3 as reference.

This formulation facilitates defining an alternate frame of reference for considering the relative vortex motion. First, choose to move with one of the vortices, say vortex $\ell$. The effect of choosing different vortices as the origin is discussed below. Now, rotate the frame so that the co-moving

location of the circumcenter,

$$\tilde{Z}(t) = \left[Z(\hat{t}) - z_\ell(\hat{t})\right] e^{-\mathrm{i}\phi_\ell(\hat{t})} = \pm R(t), \tag{4.2}$$

is purely real, moving only along the horizontal line passing through $\tilde{z}_\ell(\hat{t}) = 0$. The vortex positions in this moving frame are then given by

$$\tilde{z}_j(\hat{t}) = \left[z_j(\hat{t}) - z_\ell(\hat{t})\right] e^{-\mathrm{i}\phi_\ell(\hat{t})}. \tag{4.3}$$

For the example from regime I, the vortex motion in a frame moving according to (4.3) with $\ell = 1$ is shown in Fig. 6c. In this frame, vortex 2 oscillates along a short arc near vortex 1, with the isosceles triangles at the full and half-period times being at the extrema of this relative motion. Vortex 3 orbits clockwise along a nearly circular trajectory with a radius of approximately $2R_0$. Colinear configurations occur when the three vortices lie on a vertical line passing through $\tilde{z}_1$.

By symmetry, the overall dynamical behavior produced by initial conditions from regimes II and III is identical to that in regime I up to a rotation. However, the individual vortex motions do depend on relative position in the configuration and are therefore affected by the choice of labels. Thus, the details of the description in the co-moving frame are a function of which regime is being considered and/or which vortex is selected as the reference. Examples of this dependence are shown in Fig. 7 for representative motions in regimes II and III. Initial conditions are identical, under relabeling, to that in Fig. 6. By this relabeling, using vortex 1 as the reference for the co-moving frame, as in Figs. 7b, 7c, gives a different representation than in Fig. 6c. Regardless of which vortex is chosen as reference, at least one of the vortices orbits periodically about that reference vortex. The similarities in these representations are straightforward to determine in this symmetric case, but the direct correspondence is not necessarily obvious in general. If, in this symmetric case, the choice of reference vortex is changed, the identical co-moving representation can be produced, as illustrated in Figs. 7d, 7e.

Consider now motions from regime IV. Level curves in phase space, shown again in Fig. 8a, encircle the fixed point, with phase space trajectories orbiting counterclockwise. A representative real-space motion is shown in a fixed frame of reference in Fig. 8b for one full period of the relative motion. The vortices never become colinear in this regime, and all three vortices interact more consistently than in regimes I–III. This example highlights the value of viewing the motion in the selected co-moving frame, which transforms the somewhat complicated motion exhibited in a fixed frame to that shown in Fig. 8c. When in a frame that moves and rotates with vortex 1, vortices 2 and 3 oscillate along trajectories that trace out symmetric arcs. In this example, despite not being particularly close to the equilateral triangle equilibrium, the size of the circumcircle remains relatively consistent throughout the motion, as seen in Fig. 8c and quantified in panel (d). As vortices 2 and 3 oscillate relative to vortex 1 along their arced trajectories, the entire configuration rotates in a fixed frame at a variable rate, as shown with $\phi_1(t)$ in Fig. 8e. Comparing the co-moving trajectories in Figs. 7b–7e and in Fig. 8c clearly reveals the difference between orbiting motion in regimes I–III and tumbling motion in regime IV.

The remaining motion to consider is that along a separatrix in phase space. By way of example, take the initial position on the separatrix shown in Fig. 8a, for which $\mathbb{C} = 1/54$. As $\hat{t} \to +\infty$, the configuration becomes colinear, with $\theta_1, \theta_3 \to 0$ and $\theta_2 \to \pi$. Similarly, as $\hat{t} \to -\infty$, the configuration becomes colinear, with $\theta_2, \theta_3 \to 0$ and $\theta_1 \to \pi$; perturbing this equilibrium configuration while keeping $\tilde{H} = \text{constant}$ leads to relative vortex motion that passes through the isosceles triangle corresponding to the chosen initial condition. Vortex trajectories in a fixed frame for $0 \leqslant \hat{t} \leqslant 10$ are shown in Fig. 9d, and even in this relatively short time the configuration has approached quite close to a colinear configuration, with the circumcenter of the inscribed circle well beyond the range of panel (d). In the co-moving frame with $\ell = 1$, Fig. 9e, vortices 2 and 3 move clockwise around vortex 1 as the configuration asymptotically approaches the colinear equilibrium represented by the vertical dashed line; this equilibrium state rotates rigidly with a constant angular velocity $\mathrm{d}\phi_1/\mathrm{d}t = \mathrm{d}\phi_2/\mathrm{d}t = \mathrm{d}\phi_3/\mathrm{d}t$ and has $\rho \to \infty$ as $\hat{t} \to +\infty$, as shown in Fig. 8f. If instead $\hat{t} \to -\infty$, the vortices approach the colinear configuration given by $3_{-\infty}, 1, 2_{-\infty}$, with the notation being $j_{\hat{t}} = \tilde{z}_j(\hat{t})$; the label for vortex 1 is shown without a subscript because it is fixed in this frame. If this latter colinear configuration is perturbed with $\tilde{H} = \text{constant}$, the motion in this co-moving frame consists of vortex 3 rotating clockwise by 180° around vortex 1, while vortex 2 moves

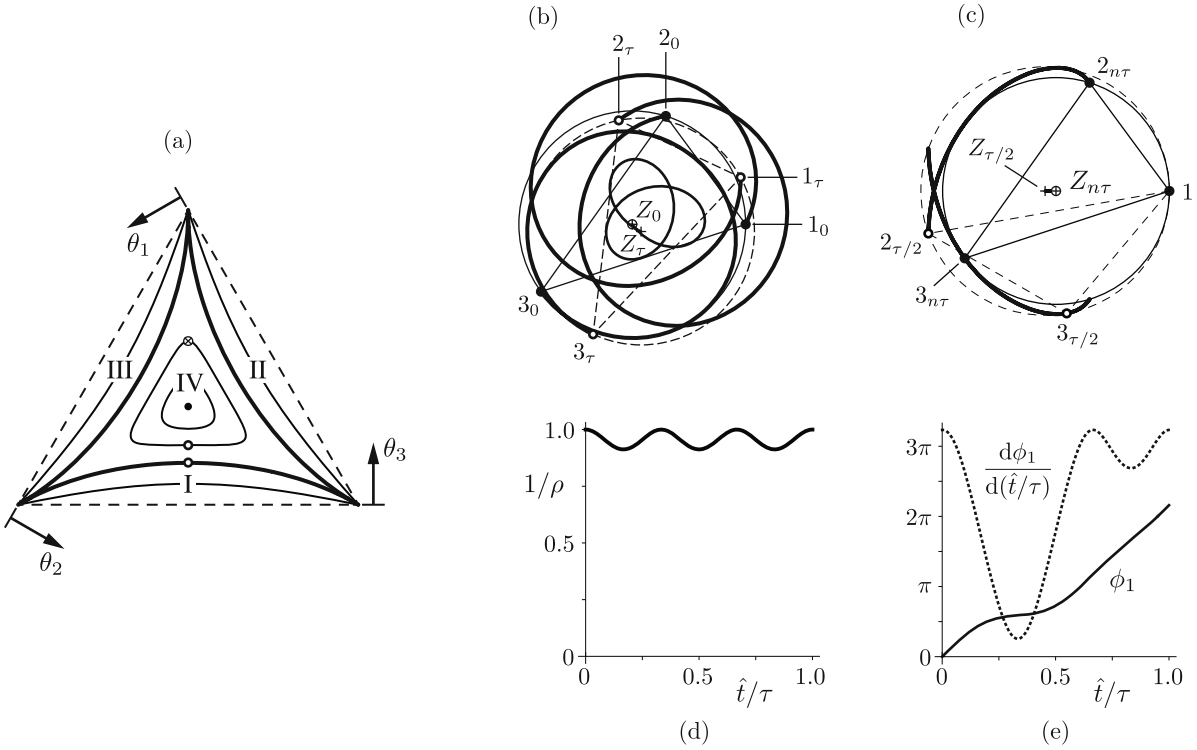


**Fig. 8.** Representative vortex trajectories from regime IV for $G_1 = G_2 = G_3 = 1$. (a) Phase space representation, with the open circle on the level curve in regime IV given by $\mathbb{C} = 1/35$ showing the initial position $\theta_3 \approx 0.635$, $\theta_1 = \theta_2 = \frac{1}{2}(\pi - \theta_3)$; half-period position is marked by $\otimes$. Open circle on the separatrix (heavy line) marks initial position for the trajectories in Fig. 8b. (b) *Tumbling* vortex trajectories (heavy solid lines) in a fixed frame of reference for one temporal period of the relative motion, $\hat{t}_f = \tau \approx 37.60$. Vortex positions $z_j(\hat{t})$ are labeled according to the index $j_{\hat{t}}$, with subscript indicating the corresponding time $\hat{t}$; initial and final positions are marked by solid and open circles, respectively. Initial and final positions of the circumcenter are marked with the symbols $\oplus$ and $+$, respectively; initial and final positions of the triangle and circumscribed circle are shown with solid lines and dashed lines, respectively. (c) Vortex and circumcenter trajectories for one period in a frame moving and rotating according to Eq. (4.3) with $\ell = 1$. Initial and final positions (after one full period) are identical for vortices (solid circles labeled $j_{n\tau}$), triangle (solid line), circumcenter ($\oplus$ labeled $Z_{n\tau}$), and circumcircle (solid line). Also shown are the vortex positions (open circles labeled $j_{\tau/2}$), the triangle and circumcircle (dashed lines), and the circumcenter ($+$ labeled $Z_{\tau/2}$) for $\hat{t} = \tau/2 + n\tau$. The full trajectory of the circumcenter is the short line bounded by $+$ and $\oplus$. (d), (e) Corresponding evolution for one temporal period of (d) the radius of the circumcircle and (e) the (rate of change of) orientation of the triangle, as given by (the temporal derivative of) $\phi_1(t)$.

counterclockwise to position $2_0$ and then returns clockwise to its initial position. The relative vortex motion along this separatrix from one equilibrium configuration to another thus corresponds to a permutation of the colinear vortex positions in infinite time.

Finally, for comparison consider small perturbations from the separatrix motion. For initial conditions, maintain $\theta_1 = \theta_2 = \frac{1}{2}(\pi - \theta_3)$ and perturb $\theta_3$ so that $\mathbb{C} = 1/53$, giving a motion in regime IV as shown in Figs. 9a–9c, or $\mathbb{C} = 1/55$, giving a motion in regime I as shown in Figs. 9g–9i. Comparing the motions for these examples with the separatrix motion in a fixed frame of reference, Figs. 9a, 9d, 9g show some initial similarities in the motion, but the comparison is best accomplished in the co-moving frame given by Eq. (4.3) with $\ell = 1$, as shown in Figs. 9b, 9e, 9h. In both regimes I and IV, vortices 2 and 3 initially orbit clockwise about (stationary) vortex 1, as in the separatrix case. In regime IV, the configuration approaches, but does not reach, a colinear state at $\hat{t} = \tau/6$, after which vortex 3 reverses direction along its path, while vortex 2 is redirected, and both vortices then begin orbiting counterclockwise about vortex 1. As shown in Fig. 9c, the vortex triangle becomes nearly colinear (producing a minimum in $1/\rho$) three times during each period of relative motion; these three states occur at $\hat{t} = (2n+1)\tau/6$, with corresponding vortex positions

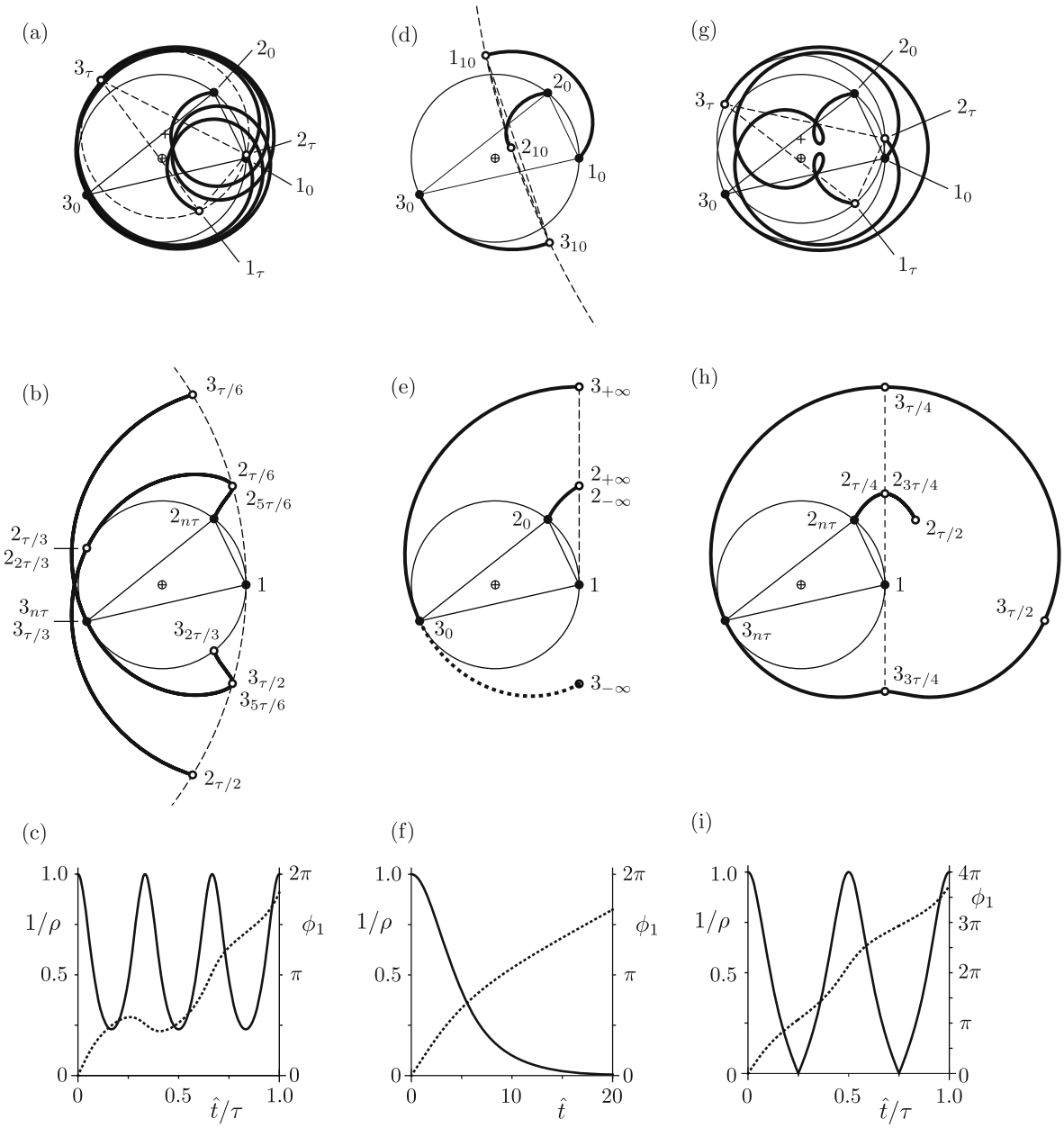


**Fig. 9.** Representative real space motions for isosceles triangle initial conditions on and near the separatrix location shown in Fig. 8a with $\theta_1 = \theta_2 = \frac{1}{2}(\pi - \theta_3)$. In panels (a)–(h), vortex positions $z_j(\hat{t})$ are labeled according to the index $j$, with subscript indicating the corresponding time $\hat{t}$; the initial and final (when relevant) circumcenter positions are shown with $\oplus$ and $+$, respectively. In panels (g)–(i), $1/\rho$ is shown with a solid line and $\phi_1$ with a dotted line. (a)–(c) Motion in regime IV with $\mathbb{C} = 1/53$ and $\theta_3 \approx 0.452$ (a) in a fixed frame of reference for one period of relative motion, $\tau \approx 57.9$, (b) in a co-moving frame with $\ell = 1$, for which the vortex motion is time-periodic; and (c) showing the corresponding evolution of $\rho$ and $\phi_1$. (d)–(f) Motion along the separatrix with $\mathbb{C} = 1/54$ and $\theta_3 \approx 0.447$ in (d) a fixed frame for $0 \leqslant \hat{t} \leqslant 10$; (e) in a co-moving frame with $\ell = 1$ as $\hat{t} \to \pm\infty$, with open circles showing the limiting vortex positions, dashed line showing the colinear configuration consisting of vortices $1, 2_{+\infty}, 3_{+\infty}$ as $\hat{t} \to +\infty$, and dotted line showing the trajectory of vortex 3 for $\hat{t} < 0$; and (f) showing the evolution of $\rho$ and $\phi_1$ for $0 \leqslant \hat{t} \leqslant 20$, with $\rho \to \infty$ and $\mathrm{d}\phi_1/\mathrm{d}t \to$ constant as $\hat{t} \to \infty$. (g)–(i) Motion in regime I with $\mathbb{C} = 1/55$ and $\theta_3 \approx 0.441$ (g) in a fixed frame of reference for one period of relative motion, $\tau \approx 37.4$; (h) in a co-moving frame with $\ell = 1$, for which the vortex motion is time-periodic and colinear states are shown with a dashed line; and (i) showing the evolution of $\rho$ and $\phi_1$, with $1/\rho = 0$ at $\hat{t} = \tau/4, 3\tau/4$. In panels (b), (h), intermediate triangles are not shown for clarity, and vortex positions at fractional periods also repeat periodically with period $\tau$.

shown in Fig. 9b. Similarly, isosceles triangle configurations occur at $\hat{t} = n\tau/3$. In regime I, on the other hand, the vortices do reach, and immediately pass through, a colinear state at $\hat{t} = \tau/4$. Both vortices continue to orbit clockwise about vortex 1 until the symmetric isosceles triangle configuration is reached at $\hat{t} = \tau/2$, at which point vortex 2 reverses direction and vortex 3 continues orbiting clockwise. Colinear states are passed through periodically at $\hat{t} = (2n+1)\tau/4$. Comparisons of Figs. 9a–9c with Figs. 8b–8e and Figs. 9g–9i with Figs. 6b–6e also show that relative vortex motions from the same regime of motion in phase space are qualitatively the same.

### *4.2. The Case $G_1 = G_2 = -G_3 = 1$ ($\Gamma_1 = \Gamma_2 = $ - $\Gamma_3$)*

As the second example, consider the case in which the vortex strengths are all the same magnitude but differ in sign. Again, assume $\Gamma_1 = \Gamma_2 > 0$, so that $G_1 = G_2 = 1$. With this choice of strengths, the symmetric functions (1.1a), (1.3) are $\gamma_1 = g_1 = 1$ and $\gamma_2 = \gamma_3 = g_2 = g_3 = -1$. The fundamental region in phase space for this case is shown in Fig. 10a. Again $g_1 \neq 0$, so almost every level curve is given by

$$\mathbb{C} = \frac{\left(\sin^2\theta_1\right)\left(\sin^2\theta_2\right)\left(\sin^2\theta_3\right)^{-1}}{\sin^2\theta_1 + \sin^2\theta_2 - \sin^2\theta_3}. \tag{4.4}$$

This equation for $\mathbb{C}$ is singular when $\sin^2(\theta_1+\theta_2) = \sin^2\theta_3 = \sin^2\theta_1 + \sin^2\theta_2$, which has the solution $\theta_3 = \pi/2$. By Eq. (3.6), this singularity is identical to taking $\tilde{L} = 0$; the corresponding level curve is shown in Fig. 10a with a dotted line. The corresponding $(b_1, b_2, b_3)$ phase space representation for this case comes from the combination of panels (b) and (c) in Fig. 2.

There are several obvious differences between the phase space representation in Fig. 10a and that from Section 4.1. First, by (3.14), $\delta = -1 < 0$ (or, alternatively, by (3.13), $D = -16 < 0$), and the equilateral triangle configuration is a saddle point in phase space. The level curves, or separatrices, passing through this point are, by Eq. (3.12), given by $\mathbb{C} = \mathbb{C}' = 1$, and inspection of Eq. (4.4) shows that these lines are given by $\theta_1 = \theta_3$ and $\theta_2 = \theta_3$. Second, every level curve except for those in regime I pass through one (or both) of the points $(\theta_1, \theta_2, \theta_3) = (\pi/2, 0, \pi/2)$ and $(\theta_1, \theta_2, \theta_3) = (0, \pi/2, \pi/2)$. Physically, these two points on the $\theta_1, \theta_2$ axes correspond to configurations in which two oppositely-signed vortices move together as a pair a distance $d \to \infty$ from the third vortex; these limiting phase space points will be referred to as *scattering points*. Finally, there are also separatrices corresponding to perturbations of a colinear equilibrium configuration, so that there are now a total of six regimes of motion labeled I–VI in Fig. 10a.

For this set of strengths, Eq. (3.25) has only one nonsingular, real-valued solution, $\zeta_1^* = -1/2$, which by (3.27) corresponds to $\mathbb{C}_1^* = -1/8$. This relative equilibrium configuration consists of equally spaced vortices on a line with the oppositely-signed vortex (here assumed to be vortex 3 with $\Gamma_3 < 0$) situated at the center, so that $\theta_3 = \pi$ and $\theta_1 = \theta_2 = 0$. Level curves given by $\mathbb{C} = \mathbb{C}_1^* = -1/8$ extend from the top phase plane vertex to the scattering points on the $\theta_1$ and $\theta_2$ axes.

Consider first motions in regime I. Similar to regime I in Fig. 5, level curves connect two colinear states at the phase space vertices, with the real space motion consisting of vortices 1 and 2 orbiting each other, while vortex 3 moves with them some distance away, such as shown in Fig. 10b. Orbiting motion from regime I in this case has been illustrated previously by Gröbli and Zhukovsky, see, for example, Fig. 2 from Ref. [6]. In contrast to the motion in Section 4.1, here regime I is bounded by separatrices passing through the center fixed point; in the previous example, the bounding separatrix passed through two colinear equilibrium points. Since the dynamics of a system tend to "slow down" in the vicinity of a fixed point, the physical behavior at these fixed points has an influence on neighboring phase space trajectories. This influence on each of the example regime I trajectories can be seen by comparing Fig. 10d with Fig. 6d or Fig. 9i. In the present case with $\Gamma_3 = -1$, the vortex configuration spends a large fraction of each period with $R \approx R_0$, indicating that the inscribed triangle remains close to the initial configuration for a relatively long time. In contrast, with $\Gamma_3 = 1$ the circumcircle radius rapidly increases from $R_0$ and spends a much greater fraction of the period near the $R \to \infty$ colinear states. Despite this differing influence of the relative equilibrium states, the fundamental similarity of relative vortex motion in an orbiting regime with $\Gamma_1 = \Gamma_2 = \pm\Gamma_3$ is revealed by considering the motion in the co-moving frame: compare Fig. 10c

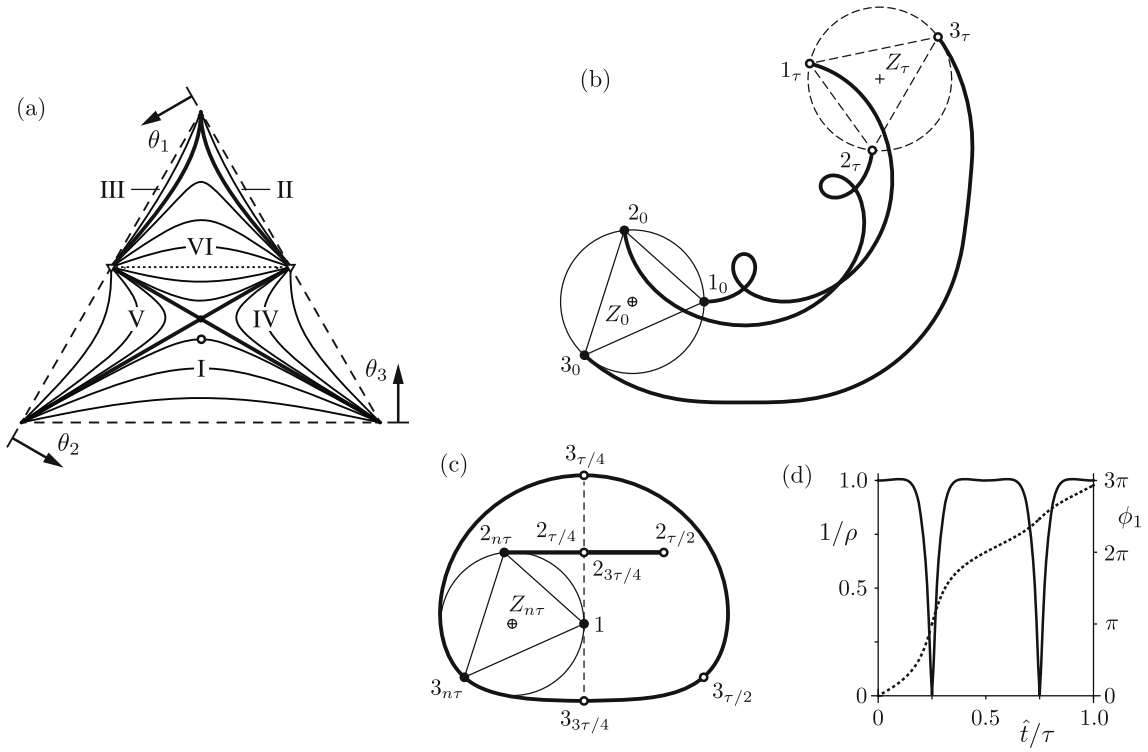


**Fig. 10.** (a) Phase space for $G_1 = G_2 = 1$, $G_3 = -1$ showing representative level curves (light lines), the curve for $L = 0$ (dotted line), and separatrices (heavy lines) that divide the phase space into 6 regimes of motion labeled I–VI. Solid circle marks the equilateral triangle location, which is a saddle point; corresponding level curves (separatrices) passing through this point have $\mathbb{C} = 1$. Triangle symbols mark the limiting cases of infinite vortex separation, termed *scattering points*. The open circle marks the point $\theta_3 \approx 0.841$, $\theta_1 = \theta_2 = \frac{1}{2}(\pi - \theta_3)$ on the curve for $\mathbb{C} = 9/8$ in regime I. Orbiting real-space motions for this initial condition in regime I are shown (b) in a fixed frame with $0 \leqslant \hat{t} \leqslant \tau \approx 53.0$, (c) in a co-moving frame with $\ell = 1$ (4.3), and (d) in terms of the radius and orientation of the circumcircle. Vortex trajectory notation is described in Fig. 6.

with Fig. 6c or Fig. 9h. In all cases, in this co-moving frame the position of vortex 2 oscillates with respect to vortex 1, while vortex 3 orbits the pair.

All other initial conditions in phase space lead to unbounded vortex motion. Next, consider motions in regimes II–V, as shown in Fig. 11. In all four of these regimes, level curves of Eq. (4.4) extend from a vertex of the fundamental triangle to the center of $\theta_1$ or $\theta_2$ axis, shown in the phase space representations by open triangle symbols. The point $\theta_1 = 0$, $\theta_2 = \theta_3 = \pi$ corresponds to a finite separation $s_1$ with $s_2, s_3 \to \infty$; that is, vortices 2 and 3 are traveling as a pair an infinite distance from vortex 1. These limiting points on the $\theta_j$ axes will be referred to as the *scattering points*. In regimes II–V, the motion consists generally of the vortex pair with strength $\pm\Gamma$ approaching the third vortex with strength $+\Gamma$, the configuration becoming colinear as the pair passes that third vortex, and then the same pair continuing on to infinity. For any initial condition in these regimes, the corresponding phase space motion approaches a scattering point as $\hat{t} \to \pm\infty$. Since the pair that comes in from and recedes to infinity contains the same vortices, this type of motion is referred to as *direct scattering*.

An example of direct scattering from regime II is shown in Figs. 11b, 11c; by symmetry, the same motion is obtained in regime III by interchanging the labels of vortices 1 and 2. In a fixed frame of reference, vortices 2 and 3 move as a pair from left to right, with vortex 1 remaining nearly stationary. To represent this motion in the co-moving frame, chose $\ell = 2$, so that the frame moves with the translating vortex pair and the identical representation is obtained for regime III by choosing $\ell = 1$ (i. e., by interchanging vortices 1 and 2). In this frame, vortex 2 is stationary, and vortex 3 has so little relative motion that it is indiscernible in the plot. The relative motion of vortex 1 progresses from left to right along what appears to be a straight line. In regimes II and III, the vortex pair is oriented so that in the colinear state the negative vortex is between

the two positive vortices. These regimes exist for only small values of $\theta_1$ (for II) or $\theta_2$ (for III); correspondingly, Fig. 2b shows that these regimes exist only for small values of $b_2$ or $b_1$, respectively. That is, direct scattering in which the oppositely-signed vortex passes closest to the third vortex requires that the pair be a significant distance from this third vortex.

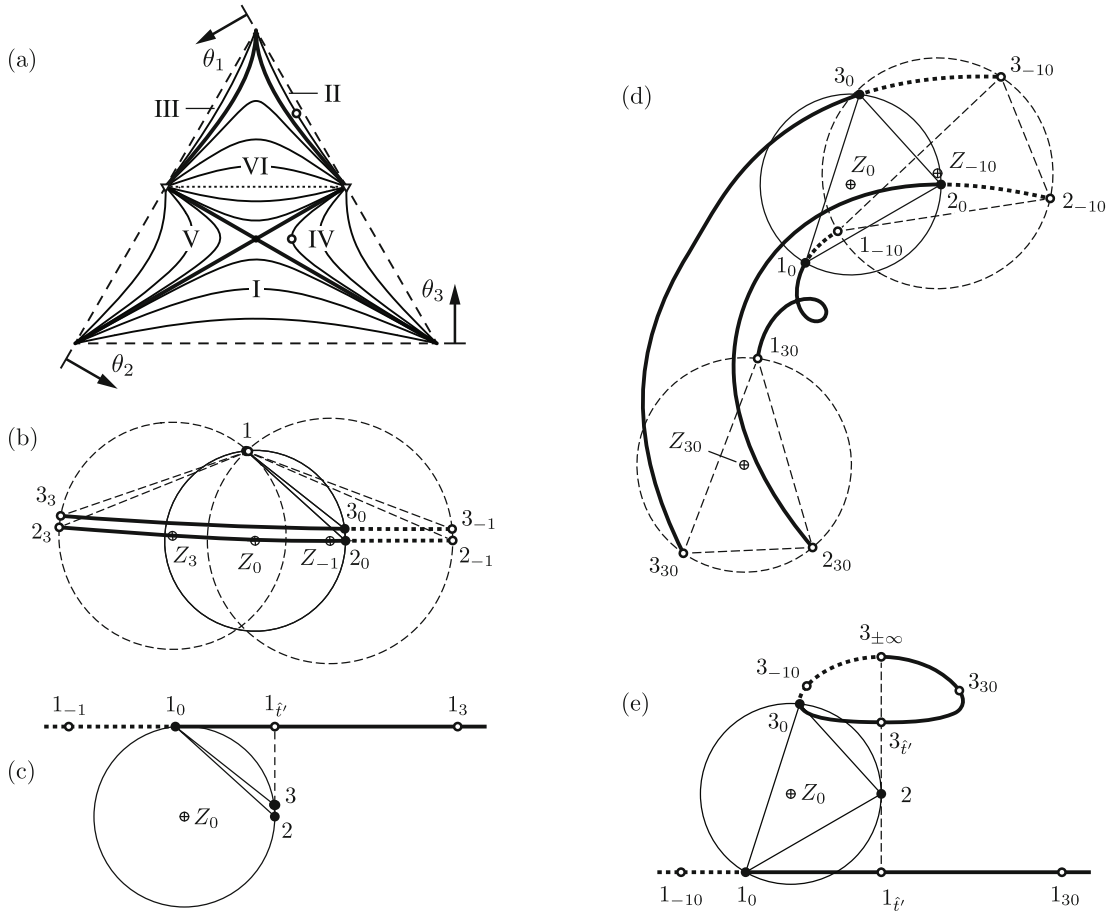


**Fig. 11.** Examples of direct scattering vortex motion for $G_1 = G_2 = 1$, $G_3 = -1$ in regimes II and IV. (a) Phase space with representative level curves. Open circles mark the initial conditions $\theta_1 \approx 0.066$, $\theta_3 = 3\theta_2 = 3(\pi - \theta_1)/4$ on $\mathbb{C} = -1/16$ in regime II and $\theta_1 \approx 0.736$, $\theta_2 \approx 1.358$, $\theta_3 = \pi/3$ on $\mathbb{C} = 7/8$. (b), (c) Real-space motions in regime II (b) in a fixed frame with $-1 \leqslant \hat{t} \leqslant 3$ and initial vortex positions chosen so that $\phi_2(0) = 0$, and (c) in a co-moving frame with $\ell = 2$ (4.3); $\tilde{x}_1 \to \pm\infty$ at $\hat{t} \to \pm\infty$. The configuration is colinear at time $\hat{t}' \approx 1.10$. The trajectory of vortex 3 is covered by the overlapping circles showing the vortex location. (d), (e) Real-space motions in regime IV (b) in a fixed frame with $-10 \leqslant \hat{t} \leqslant 30$ and initial vortex positions chosen so that $\phi_2(0) = 0$, and (c) in a co-moving frame with $\ell = 2$ (4.3). The configuration is colinear at time $\hat{t}' \approx 11.47$, and vortices 2 and 3 are aligned vertically at $\hat{t} \to \pm\infty$. All trajectories for $\hat{t} < 0$ are shown with dotted lines Notation follows Fig. 6.

An example of direct scattering from regime IV is shown in Figs. 11d, 11e; again by symmetry, the same motion is obtained in regime V by interchanging the labels of vortices 1 and 2. In this version of direct scattering, in the colinear state the two like-signed vortices are adjacent. With this vortex arrangement, direct scattering is obtained for much stronger interaction of the pair with the third vortex, and the vortex pair shows a much greater change in its net translational motion as a result of the scattering interaction. For the co-moving frame, again take $\ell = 2$, which gives the relative motion in Fig. 11e. Vortex 1 again progresses from left to right along what is essentially a straight line, but in this case it passes below the pair instead of above. The relative motion of vortex 3 is much larger in this case, forming a closed curve above vortex 2 in infinite time.

Finally, consider motions from regime VI, with representative examples shown in Fig. 12. The choice is made here to identify the areas labeled VIa, VIb, and the dotted line corresponding to

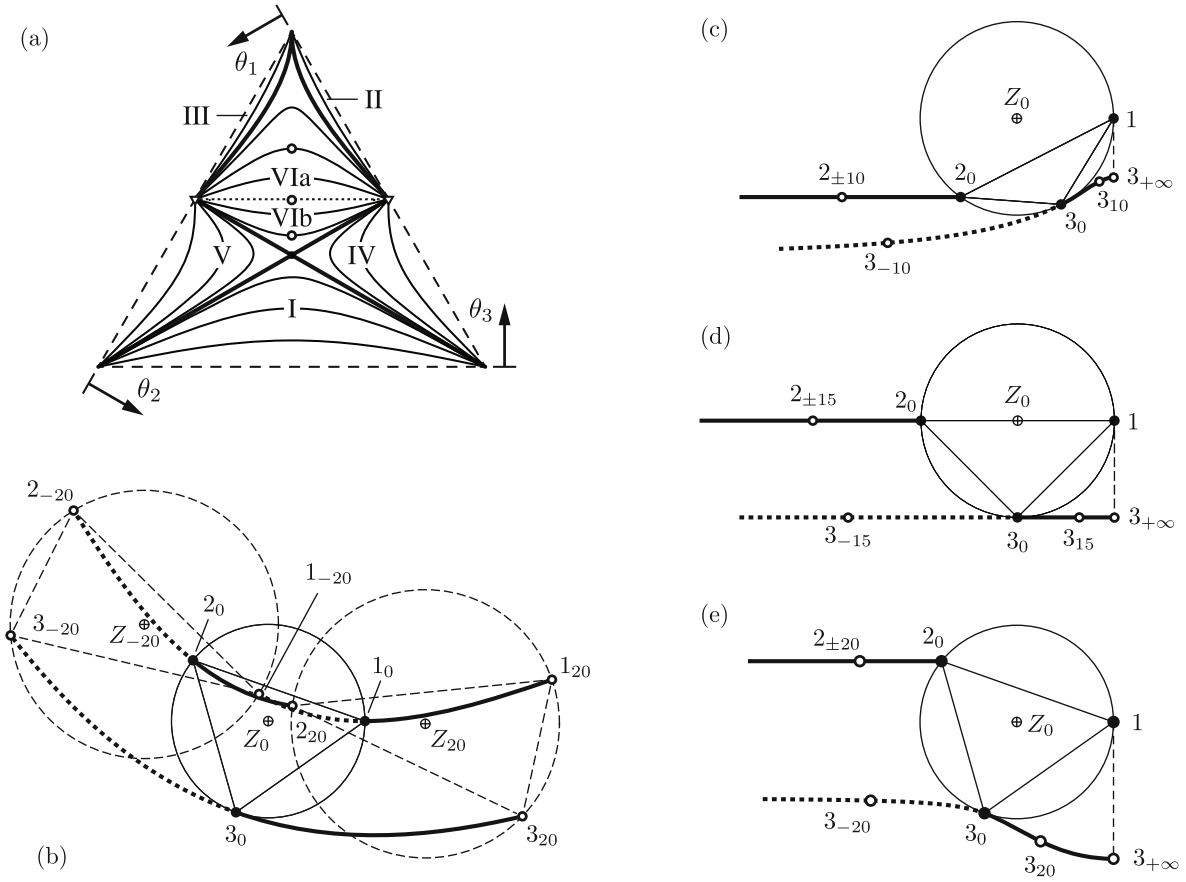


**Fig. 12.** Examples of exchange scattering vortex motion for $G_1 = G_2 = 1$, $G_3 = -1$ in regime VI. (a) Phase space representation with open circles marking example initial conditions $\theta_1 = \theta_2 = (\pi - \theta_3)/2$ and, from top to bottom, $\theta_3 \approx 2.046$ on $\mathbb{C} = -3/8$, $\theta_3 = \pi/2$ on $\tilde{L} = 0$, and $\theta_3 \approx 1.231$ on $\mathbb{C} = 9/8$. (b) Real-space motions in a fixed frame for $\theta_3 \approx 1.231$ on $\mathbb{C} = 9/8$ with $-20 \leqslant \hat{t} \leqslant 20$ and initial vortex positions chosen so that $\phi_2(0) = 0$. (c)–(e) Real-space motions in a co-moving frame with $\ell = 1$ for (c) $\theta_3 \approx 2.046$ on $\mathbb{C} = -3/8$, (d) $\theta_3 = \pi/2$ on $\tilde{L} = 0$, and (e) $\theta_3 \approx 1.231$ on $\mathbb{C} = 9/8$. All trajectories for $\hat{t} < 0$ are shown with dotted lines.

$\tilde{L} = 0$ as all belonging to the same regime of motion. The corresponding representation in $(b_1, b_2, b_3)$ phase space consists not only of two separate regions in Fig. 2b but also of the separate singular representation for $\tilde{L} = 0$ in Fig. 2c. In regime VI, all phase space level curves connect the two scattering points, so that the pairs translating together as $\hat{t} \to \pm\infty$ consist of different vortices, as illustrated by the real space motion shown in Fig. 12b. Thus, this regime consists of what is referred to as *exchange scattering*. Three different examples are shown in the co-moving frame with $\ell = 1$ for this regime in Figs. 12c–12e: one from area VIa, one for $\tilde{L} = 0$, and one from area VIa. In the frame moving and rotating with vortex 1, vortices 2 and 3 translate as a pair from left to right, with vortex 2 traveling along what appears to be a straight line. When the three vortices are located at the vertices of an isosceles triangle, identified here as the initial condition at $\hat{t} = 0$, the exchange is made, and for $\hat{t} > 0$ vortices 1 and 3 move together as a pair. In the co-moving frame, vortex 2 reverses its direction for $\hat{t} > 0$ and moves to the left along the same path as earlier, while vortex 3 moves to a location directly below vortex 1 as $\hat{t} \to +\infty$. As shown explicitly in panel (b) and can be seen by connecting the various vortex locations in panels (c)–(e), the incoming and outgoing vortex configurations form similar triangles at times $\hat{t} = \pm T$ if $\hat{t} = 0$ is taken to be the isosceles triangle configuration. The similarity between these three cases justifies the choice of identifying them as all belonging to the same regime of motion, despite the fact that taking $\tilde{L} = 0$ corresponds to a singularity in the definition of the level curves as given by (4.4). When $\tilde{L} = 0$, vortex 2 moves

directly at vortex 1; for initial conditions from area VIa (VIb), the trajectory of vortex 2 is below (above) vortex 1 in the co-moving frame.

## 5. SUMMARY

The problem of three point vortices interacting in the plane has a long, rich history of analysis. Despite the fact that the system is integrable and the degree of attention this problem has received, it would seem that a fresh perspective based on the angles of the vortex triangle can provide further insight into the details of the relative vortex motion. By representing the motion in terms of these angles, instead of using the inter-vortex separations, the phase plane topology can be represented in the same bounded domain for all cases, facilitating comparative analysis across different cases. The relative motion of the vortices and the circumcircle inscribing the vortex triangle also provide a natural frame of reference for characterizing the vortex motions. For the two canonical examples presented, in this co-moving frame the relative vortex motions follow relatively simple trajectories, with one of the vortices fixed and the other two translating, oscillating, or orbiting along simple curves. This frame highlights the similarities and differences between relative motions in different regimes.

For the examples considered with $\Gamma_1 = \Gamma_2 = \pm\Gamma_3$, the relative vortex motions can be classified into a total of six unique regimes of motion. With $\Gamma_1 = \Gamma_2 = \Gamma_3$ there are two unique regimes. The identical (under symmetry) regimes I–III consist of orbiting motion; in a co-moving frame of reference, one of the vortices orbits around the other two. Regime IV consists of tumbling motion, in which the three vortices maintain their counterclockwise orientation, oscillating in their relative positions, while the vortex triangle rotates and translates. With $\Gamma_1 = \Gamma_2 = -\Gamma_3$ there are four unique regimes. Regime I consists again of orbiting motion, and the characteristics of the relative motion in the orbiting regimes are quite consistent for $\Gamma_3 = \pm 1$. In the remainder of the regimes, a vortex pair travels to/from infinity. Symmetric regimes II–III and symmetric regimes IV–V all consist of direct scattering, with the same two vortices in the translating pair for all time. The two regimes are distinguished by whether the translating pair is oriented so that the negative vortex (II–III) or the positive vortex (IV–V) is closest to the third (positive) vortex. Regime VI contains the special case $\tilde{L} = 0$, the motions consist of exchange scattering, with the pairing of the negative vortex passing from one positive vortex to the other when the three vortices interact.

As the symmetries in this planar three-vortex system are broken by considering unequal vortex strengths, the complexity of the topology in phase space increases and additional types of relative motion become possible. This formulation provides an additional tool for characterizing the rich dynamics in this classic problem.

## CONFLICT OF INTEREST

The author declares that he has no conflicts of interest.

## REFERENCES

1. Aref, H., Motion of Three Vortices, *Phys. Fluids,* 1979, vol. 22, no. 3, pp. 393–400.
2. Aref, H., Addendum: "Three-Vortex Motion with Zero Total Circulation" [*Z. Angew. Math. Phys.,* 1989, vol. 40, no. 4, pp. 473–494] by N. Rott, *Z. Angew. Math. Phys.,* 1989, vol. 40, no. 4, pp. 495–500.
3. Aref, H., A Transformation of the Point Vortex Equations, *Phys. Fluids,* 2002, vol. 14, pp. 2395–2401.
4. Aref, H., Point Vortex Dynamics: A Classical Mathematics Playground, *J. Math. Phys.,* 2007, vol. 48, no. 6, 065401, 23 pp.
5. Aref, H., Stability of Relative Equilibria of Three Vortices, *Phys. Fluids,* 2009, vol. 21, no. 9, 094101, 22 pp.
6. Aref, H., Rott, N., and Thomann, H., Gröbli's Solution of the Three-Vortex Problem, *Annu. Rev. Fluid Mech.,* 1992, vol. 24, pp. 1–20.
7. Borisov, A. V. and Lebedev, V. G., Dynamics of Three Vortices on a Plane and a Sphere: 2. General Compact Case, *Regul. Chaotic Dyn.,* 1998, vol. 3, no. 2, pp. 99–114.
8. Borisov, A. V. and Pavlov, A. E., Dynamics and Statics of Vortices on a Plane and a Sphere: 1, *Regul. Chaotic Dyn.,* 1998, vol. 3, no. 1, pp. 28–38.
9. Coxeter, H. S. M., *Introduction to Geometry,* 2nd ed., New York: Wiley, 1989.
10. Gröbli, W., Spezielle Probleme über die Bewegung geradliniger paralleler Wirbelfäden, *Vierteljschr. Naturf. Ges. Zürich,* 1877, vol. 22, pp. 37–81, 129–165.

11. Kimura, Y., Similarity Solution of Two-Dimensional Point Vortices, *J. Phys. Soc. Japan,* 1987, vol. 56, no. 6, pp. 2024–2030.
12. Krishnamurthy, V. S., Aref, H., and Stremler, M. A., Evolving Geometry of a Vortex Triangle, *Phys. Rev. Fluids,* 2018, vol. 3, no. 2, 024702, 17 pp.
13. Krishnamurthy, V. S. and Stremler, M. A., Finite-time Collapse of Three Point Vortices in the Plane, *Regul. Chaotic Dyn.,* 2018, vol. 23, no. 5, pp. 530–550.
14. Makarov, V. G., Group Scattering of Point Vortices on an Unbounded Plane, *J. Fluid Mech.,* 2021, vol. 911, A24, 23 pp.
15. Newton, P. K., *The N-Vortex Problem: Analytical Techniques,* Appl. Math. Sci., vol. 145, New York: Springer, 2001.
16. Novikov, E. A., Dynamics and Statistics of a System of Vortices, *JETP,* 1975, vol. 41, no. 5, pp. 937–943; see also: *Zh. Èksper. Teoret. Fiz.,* 1975, vol. 68, no. 5, pp. 1868–1882.
17. Novikov, E. A. and Sedov, Yu. B., Vortex Collapse, *JETP,* 1979, vol. 50, no. 2, pp. 297–301; see also: *Zh. Èksper. Teoret. Fiz.,* 1979, vol. 77, no. 2, pp. 588–597.
18. Synge, J. L., On the Motion of Three Vortices, *Canad. J. Math.,* 1949, vol. 1, pp. 257–270.
19. van Heijst, G. J. F., Kloosterziel, R. C., and Williams, C. W. M., Laboratory Experiments on the Tripolar Vortex in a Rotating Fluid, *J. Fluid Mech.,* 1991, vol. 225, pp. 301–331.
20. von Helmholtz, H., Über Integrale der hydrodynamischen Gleichungen, welche den Wirbelbewegungen entsprechen, *J. Reine Angew. Math.,* 1858, vol. 55, pp. 25–55.
21. Wang, M. and Hemati, M. S., Detecting Exotic Wakes with Hydrodynamic Sensors, *Theor. Comput. Fluid Dyn.,* 2019, vol. 33, nos. 3–4, pp. 235–254.